https://doi.org/10.5194/egusphere-2026-1520
Preprint. Discussion started: 8 May 2026

TOPAZ5: A high-resolution ocean and sea-ice model for the Arctic and North Atlantic.

Achref Othmani[1], Annette Samuelsen[1] Jiping Xie[1], Laurent Bertino[1], Fabio Mangini[1], Roshin P. Raj[1]

[1]Nansen Environmental and Remote Sensing Centre and Bjerknes Centre for Climate Research, Bergen, Norway

Correspondence to: Achref Othmani (achref.othmani@nersc.no)

Abstract. Accurate simulation of coupled ocean-sea ice dynamics is important for understanding Arctic climate variability. This paper evaluates TOPAZ5, a novel high-resolution (6-10 km) hindcast configuration of the HYCOM-CICE model optimized for the Arctic and North Atlantic, over the period 2009-2019. TOPAZ5 is validated against satellite altimetry, in situ observations, and reanalysis products, assessing sea surface temperature (SST), sea surface salinity (SSS), sea level anomaly (SLA), eddy kinetic energy (EKE), mixed layer depth (MLD), volume transports, and sea ice properties. TOPAZ5 captures the large-scale spatial patterns of SST and SSS with strong agreement relative to the OSTIA dataset and WOA climatology; however, persistent warm and saline surface biases remain, particularly during summer and over Arctic shelf regions. SLA trends are generally consistent with satellite altimetry and reanalyses, though positive anomalies in the Norwegian and Barents Seas are underestimated. Compared to observations, the model reproduces similar spatial patterns of EKE but underestimates their amplitude, especially in the Lofoten Basin and Labrador Sea. MLD variability shows reasonable agreement with observed seasonal stratification, though the model tends to produce overly deep winter mixing in the Labrador Sea. Sea ice seasonality is well represented, but the model overestimates the central Arctic thickness and underrepresents spatial and temporal variability in marginal ice zones. While volume transports through the Bering Strait are realistically simulated, the flows through the Fram Strait and Barents Sea Opening are underestimated. Overall, TOPAZ5 demonstrates sufficient skill in simulating large-scale hydrography and sea ice dynamics to support operational forecasting applications in the North Atlantic and Arctic.

1 Introduction

The North Atlantic and Arctic regions play a critical role in global climate dynamics, as they influence ocean circulation, heat distribution, and atmospheric conditions (Timmermans et al., 2020; Smedsrud et al., 2022; Hordoir et al., 2022; Rudels and Carmack, 2022; Shi et al., 2024). These regions drive the Atlantic Meridional Overturning Circulation (AMOC), which shapes climate patterns across the Northern Hemisphere (Buckley et al., 2016; Weijer et al., 2019; Hassan et al., 2021). Characterized by complex interactions between ocean waters and sea ice, they significantly affect weather systems, marine ecosystems, the global energy budget, carbon exchange, and climate feedback.

https://doi.org/10.5194/egusphere-2026-1520
Preprint. Discussion started: 8 May 2026

High-resolution modelling of ocean and sea ice dynamics is therefore essential to understand long-term changes. However, simulating these regions remains challenging due to the intricate coupling of atmospheric, oceanic, and sea ice processes (Docquier et al., 2019; Fine et al., 2023; Selivanova et al., 2024). Key uncertainties stem from difficulties in capturing mesoscale processes and extreme events (Dorn et al., 2007; Hewitt et al., 2020; Zhou et al., 2023), compounded by sparse observational data that hinder validation and necessitate advanced data assimilation techniques (Carrassi et al., 2018).

Several regional models have already been validated for the Nordic Seas and Arctic and use in their majority advanced models in Cartesian vertical coordinates, notably ASTE (Nguyen et al., 2021), NEMO (Hordoir et al., 2019), RIOPS (Smith et al., 2024), and FESOM (Wang et al., 2018), but less so the isopycnic and hybrid vertical coordinate models. Even the latter often resort to using Cartesian vertical levels in high latitudes (Dukhovskoy et al., 2009). The use of isopycnic coordinates is advantageous for ensemble data assimilation (Counillon et al. 2016), which again favours coupled ice-ocean data assimilation (Sakov et al. 2012) and coupled physical-biogeochemical modelling, both important features of Arctic Ocean forecast and reanalysis products.

To address these issues, the TOPAZ5 system provides a state-of-the-art, coupled ocean-sea ice modelling framework in hybrid vertical coordinates throughout the whole Arctic. TOPAZ5 is intended to analyse past ocean and ice variability and includes an operational forecasting version that integrates advanced data assimilation to enhance predictive skill like its predecessor TOPAZ4 (Xie et al. 2017). This study evaluates the performance of TOPAZ5 in simulating ocean and sea ice dynamics in the North Atlantic and Arctic. The work is part of ongoing efforts to improve regional ocean forecasting and reanalysis capabilities. The results help refine TOPAZ5's parameterizations and enhance its ability to reproduce observed conditions in these vulnerable high-latitude environments. Unlike TOPAZ4, which included ensemble data assimilation, the present TOPAZ5 configuration is evaluated in free-running mode. This allows us to isolate model biases prior to introducing observational constraints.

2 Material and methods

TOPAZ5 configuration is a coupled ocean and sea ice modelling system for the North Atlantic and the Arctic Ocean. TOPAZ5 is based on version 2.2.98 of the HYbrid Coordinate Ocean Model, HYCOM (Bleck, 2002) and version 5.1 of the Los Alamos sea ice model (CICE, Hunke et al., 2015). HYCOM, uses the tracer and continuity equation solved with the second order flux corrected transport (FCT2, Iskandarani et al., 2005; Zalesak, 1979). It uses a hybrid vertical coordinate system, combining isopycnals with z-level and sigma coordinates, our configuration combines only isopycnal and z-level coordinates. TOPAZ5 uses vertical remapping for isopycnal coordinate layers using the Weighted Essentially Non-Oscillatory (WENO) piecewise parabolic method, and the vertical mixing is defined by the K-Profile Parameterization scheme (Large et al., 1994). The short-wave radiation penetration is implemented with varying exponential decay depending on the Jerlov water type based on a monthly climatology of satellite-derived attenuation of photosynthetically available radiation (Kara et al., 2005).

https://doi.org/10.5194/egusphere-2026-1520
Preprint. Discussion started: 8 May 2026

The sea ice model, CICE 5.1, consists of modular interacting components for thermodynamics, ice dynamics, ice transport, and a ridging parameterization. The thermodynamic component in CICE is computed by the local rates of change of snow and ice due to vertical conductive, radiative, and turbulent fluxes, along with snowfall with the rule of conserving energy (Bitz et al., 2001; Turner et al., 2013). The sea ice dynamics uses the elastic-viscous-plastic (EVP) rheology to account for the deformation of the ice pack (Hunke and Dukowicz, 1997; Hunke, 2001). The transport module describes the advection of the areal concentration, ice volumes, and other ice state variables. The ridging parameterization computes the ice transfer between different thickness categories based on energetic balances and rates of strain. In the present configuration of CICE, a linear function of salinity (Bitz and Lipscomb 1999) is used for the freezing temperature, and the sea ice ridging is calculated based on Hibler (1980) method. The shortwave radiation scheme uses the Delta-Eddington approximation, where the snow and sea ice albedo are tuned based on the inherent optical properties of snow and bare ice. In addition, the effect of melt pond on level ice is parameterized during radiation calculation, but there is no explicit tracking of melt ponds. The HYCOM-CICE coupling (exchange of stress, heat, salinity) is accomplished through the Earth System Modelling Framework (ESMF, version 8.0.1).

TOPAZ5 grid covers the Arctic, the North Atlantic Oceans and a small region of the North Pacific Ocean to account for the flow through the Bering Strait (BS, Fig. 1).

https://doi.org/10.5194/egusphere-2026-1520
Preprint. Discussion started: 8 May 2026

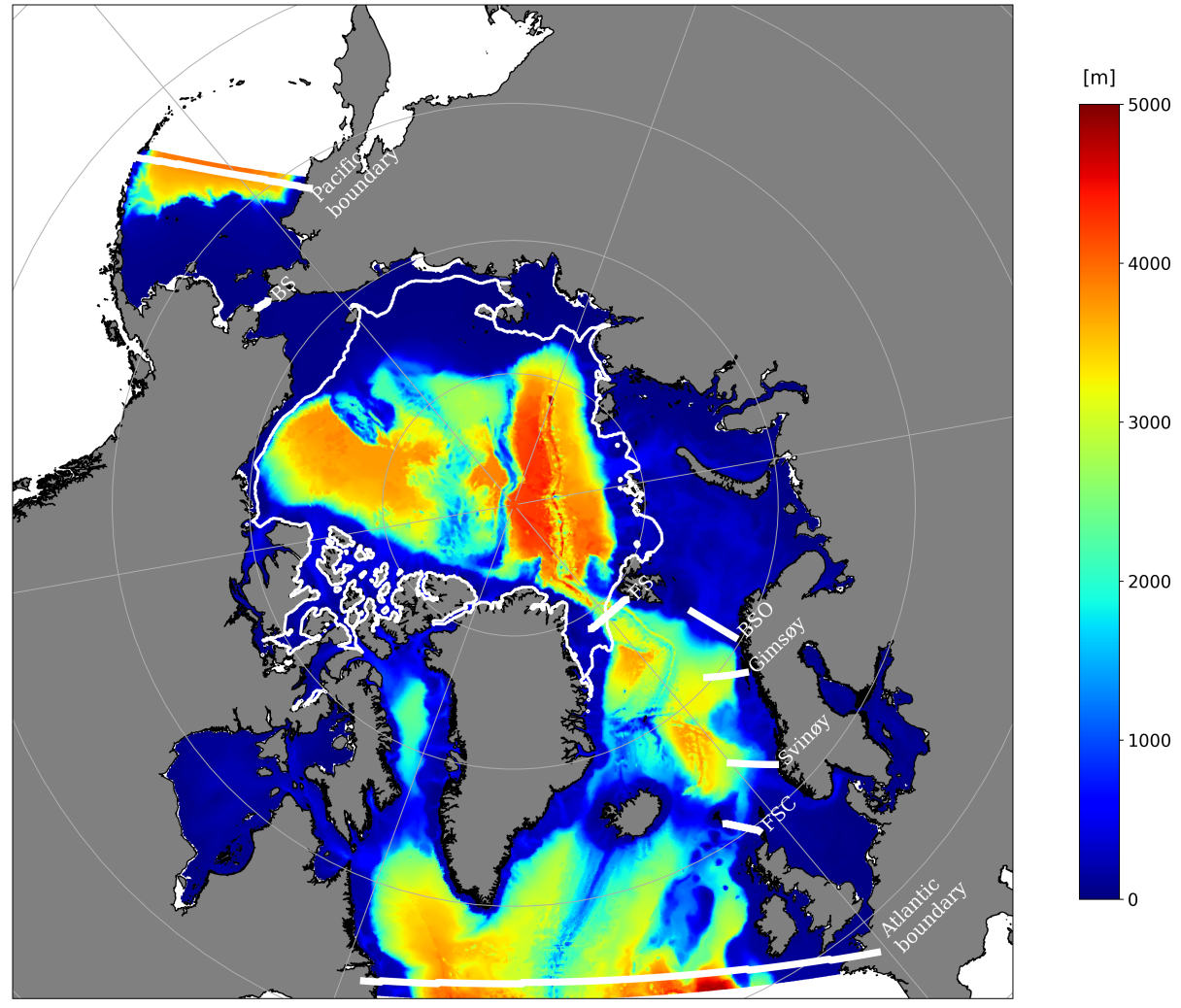

Fig. 1. TOPAZ5 model domain and bathymetry (m). Validation sections are shown as white lines: Faroe-Shetland Channel (FSC), Svinøy, Gimsøy, Barents Sea Opening (BSO), Fram Strait (FS), and Bering Strait (BS). The central Arctic area within the white contour is excluded from region-wide temperature and salinity time series. Pacific and Atlantic domain boundaries are indicated along the corresponding edges.

TOPAZ5 has a horizontal resolution varying from 6.4 km at the Pacific boundary to 10.2 km at the Atlantic boundary which resolves the large meso-scale variability in the ocean and sea ice. In the vertical, TOPAZ5 is configured with 50 layers, the 10 upper layers are always z-levels, and the top layer is 1.2 m. The target densities for the lower 40 hybrid z-layers were adjusted to reflect the water masses in the focus region. The barotropic and baroclinic time steps are 15 seconds and 5 minutes, respectively. The bathymetry is based on the General Bathymetric Chart of the Ocean (GEBCO_2014, https://www.gebco.net/). The model atmospheric forcing fields (precipitation, dew point temperature, air temperature at 2 m, sea level pressure, surface winds, long and short-wave radiation at the sea surface) are from the ERA5 reanalysis (Hersbach

https://doi.org/10.5194/egusphere-2026-1520
Preprint. Discussion started: 8 May 2026

et al., 2020) from the European Centre for Medium-Range Weather Forecasts. The atmospheric forcing has a 6-hourly frequency. Wind stress and heat fluxes are estimated using COARE 3.0 algorithm (Fairall et al, 2003). The river runoff was calculated using a combination of monthly climatology from the Arctic-HYPE and E-HYPE hydrographic models developed by the Swedish Meteorological and Hydrological Institute (SMHI; Lindström et al., 2010), as well as data from the Total Runoff Integrating Pathways (TRIP; Oki and Sud, 1998). This calculation also incorporates freshwater contributions from the Greenland Ice Sheet mass loss (Groh et al., 2019). Time series data from eight drainage basins were analysed using linear regression, and the resulting regression slopes were converted into freshwater fluxes. These fluxes were subsequently distributed across estuaries along the Greenland coast.

A hindcast simulation using TOPAZ5 was conducted for the period from 1992 to 2019. The model was initialized from rest in September 1992, utilizing temperature and salinity fields from the World Ocean Atlas 2018 (WOA 2018) climatology (Locarnini et al., 2019; Zweng et al., 2019). During 1992, temperature and salinity were relaxed towards the corresponding monthly climatology from WOA 2018 at the lateral boundaries. This relaxation was implemented using zones with a width of twenty grid cells and a relaxation timescale of twenty days. In addition, surface relaxation of sea surface salinity (SSS) towards the corresponding monthly climatology was applied.

From 1993 onwards, nesting conditions were applied at the lateral boundaries using data from the GLORYS 12 V1 reanalysis (daily outputs at 1/12° horizontal resolution, 50 vertical levels, https://doi.org/10.48670/moi-00021). The nesting process involved relaxation zones with a width of twenty grid cells and a relaxation timescale of one day. This approach was applied to temperature, salinity, horizontal ocean currents, and pressure, with the barotropic pressure at the open boundaries computed from sea surface height (SSH) and the Montgomery potential. A spatially variable formulation is used for the thickness and velocity diffusion with an increased value in the nesting zone to damp instabilities. The model results were saved as daily means. The first 17 years were considered a spin-up phase and the model's performance was evaluated for the 2009-2019 period. The hindcast simulation described here uses no data assimilation. All results reflect the intrinsic performance of the HYCOM-CICE coupling.

2.1 Validation datasets

The modelled Sea Surface Temperature (SST) fields are compared to the Operational Sea Surface Temperature and Sea Ice Analysis, OSTIA dataset (daily temporal resolution at 0.05° x 0.05° horizontal grid resolution, https://doi.org/10.48670/moi-00165) from the UK's Met Office (Donlon et al., 2012). Additionally, the model SST and Sea Surface salinity (SSS) fields are compared to the World Ocean Atlas, WOA 2018 representing the period from December 2005 to 2017 (NOAA product at 0.25° x 0.25° grid resolution) temperature (Locarnini et al., 2019) and salinity (Zweng et al., 2019) climatologies.

For the analysis of SST and SSS time series, regions with monthly sea ice concentrations exceeding 15% were excluded due to the limited data coverage beneath sea ice. This masking effectively restricts the domain of the analysis to the ice-free Arctic.

https://doi.org/10.5194/egusphere-2026-1520
Preprint. Discussion started: 8 May 2026

The model outputs are compared to hydrographic observations from the sections at Svinøy, Gimsøy and BSO (Fig. 1) provided by the Norwegian Institute of Marine Research. These sections are sampled 4-6 times a year, we have used observations from 2009-2019 to compute seasonal estimates that were compared to the model. The chosen sections cross the main gateways between the Nordic Seas and adjacent areas and capture the Atlantic Water (AW) flowing northward along the Norwegian continental slope.

For the sea level anomaly (SLA) and eddy kinetic energy (EKE), the model outputs were compared to satellite observations (0.25° × 0.25° spatial resolution) obtained from the E.U. Copernicus Marine Service Information; https://doi.org/10.48670/moi-00148. Grid cells not covered by the Altimetry data were masked in TOPAZ5 and GLORYS to ensure a consistent comparison across datasets. This masking procedure defines the Altimetry domain, ensuring uniform data coverage. The model Mixed Layer Depth (MLD) is validated against a global climatology dataset of MLD computed from observations. The criterion selected is a constant density threshold of 0.03 kg/m3, and a surface reference depth fixed at 10 m (de Boyer Montégut et al., 2004).

The modelled sea ice thickness is compared to the CS2SMOS dataset (Ricker et al., 2017), which integrates CryoSat-2 radar altimetry and SMOS sea ice thickness from passive microwave radiometry (spatial resolution of 25 km). The modelled sea ice concentration is compared to the Ocean and Sea Ice Satellite Application Facility (OSI SAF) dataset (spatial resolution of 25 km), available at https://doi.org/10.15770/EUM_SAF_OSI_0012 (OSI SAF, 2022).

2.2 Validation metrics

In this study, we use the temporal standard deviation of SSH as a proxy for the time-mean eddy kinetic energy (EKE), following established methodologies (Stammer, 1997; Volkov et al., 2013; Jiang et al., 2023). Under geostrophic balance, enhanced SSH variability corresponds to stronger horizontal gradients, higher geostrophic velocities, and thus increased EKE. Therefore, the SSH standard deviation provides a robust proxy for identifying regions of intensified mesoscale and sub mesoscale variability, such as boundary currents and inflow regions (Volkov et al., 2013; Juricke et al., 2020; Schubert et al., 2023).

To quantify the misfits between the model and available observations, we compute the bias and root mean square error (RMSE). The bias is defined as:

$$Bias = \frac{1}{N}\sum_{i=1}^{N}\left(X_{mod,i} - X_{obs,i}\right), \quad (1)$$

and the RMSE as:

$$RMSE = \sqrt{\frac{1}{N}\sum_{i=1}^{N}(X_{mod,i} - X_{obs,i})^2}, \quad (2)$$

where $X_{mod,i}$ and $X_{obs,i}$ denote the modelled and observed variables at time index i, respectively, and N is the total number of samples. Bias is consistently defined as model minus observation throughout the study.

https://doi.org/10.5194/egusphere-2026-1520
Preprint. Discussion started: 8 May 2026

3 Results

3.1 Basin-scale hydrography

3.1.1 Surface temperature

The spatial distribution of TOPAZ5 SST during winter (January to March) and summer (July to September) for the period 2009-2019, together with a comparison to OSTIA observations, is shown in Fig. 2.

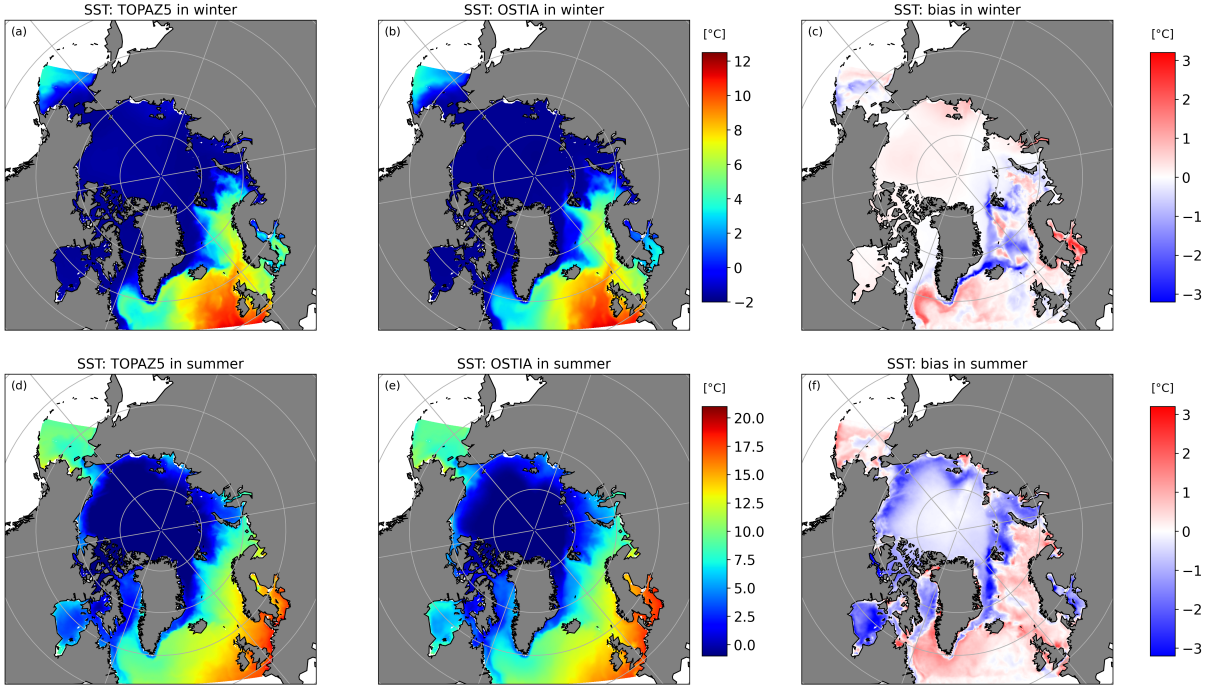

Fig. 2. Maps of the SST means in winter (a, b) and summer (d, e) from TOPAZ5 and OSTIA, and their difference (Model - OSTIA) (c, f). Seasonal means are computed over January-March (winter), and July-September (summer) for 2009-2019.

The SST fields (Fig. 2) indicate the presence of Atlantic Water (AW; temperature > 5 °C and salinity > 35) in the mid-latitude North Atlantic, crossing the Greenland-Scotland Ridge and entering the Nordic Seas. Cold Polar Water (PW; temperature < 2 °C) is evident in the western Fram Strait and along the East Greenland Current toward the Labrador Sea.

In winter, the SST bias map (Model - OSTIA, Fig. 2c) shows a warm bias of about 2 °C following the Labrador Current and a cold bias of about 2 °C in the East Greenland Current, extending into the eastern Nordic Seas toward the Norwegian and Lofoten Basins. The Greenland Sea exhibits a warm bias of approximately 1 °C, whereas regions south of Svalbard and in the Denmark Strait show a cold bias of around 1 °C. The Norwegian Sea exhibits both cold and warm biases.

https://doi.org/10.5194/egusphere-2026-1520
Preprint. Discussion started: 8 May 2026

In summer (Fig. 2f), a warm bias appears in the Labrador Sea, Norwegian Sea and Barents Sea. A cold bias of about 2-3 °C is present around the marginal ice zone (MIZ) and about 1 °C in the central Arctic Ocean, Greenland Sea, Beaufort Sea and Laptev Sea.

Basin-averaged statistics, excluding the ice-covered Arctic, for the period 2009-2019 indicate that SST in TOPAZ5 is closer to OSTIA dataset (RMSE = 0.17 °C, Bias = -0.11 °C) than to the WOA climatology (RMSE = 0.43 °C, Bias = -0.35 °C) (Table 1). The small bias relative to OSTIA, together with the low RMSE, indicates that the model captures the mean state well and shows good agreement with observed variability. The larger RMSE relative to WOA reflects the difference between a dynamically varying model and a climatological reference that does not include interannual variability. The SST trend over the analysis period is 0.068 °C yr^{-1} in TOPAZ5 and 0.062 °C yr^{-1} in OSTIA, indicating close agreement in the simulated warming rate.

Table 1: Summary of the modelled SST and SSS trends, associated bias and root mean square error (RMSE) compared with OSTIA and WOA for the period 2009-2019.

	Trend TP5 (yr^{-1})	Trend OSTIA (yr^{-1})	Bias vs OSTIA	Bias vs WOA	RMSE vs OSTIA	RMSE vs WOA
SST (°C)	0.068	0.062	-0.11	-0.35	0.17	0.43
SSS	-0.008	-	-	-0.21	-	0.24

3.1.2 Surface salinity

Together with the SST patterns described above, the SSS fields help distinguish Atlantic Water (AW; salinity > 35) from Polar Water (PW; salinity < 34). The spatial distribution of SSS from TOPAZ5 is shown in Fig. 3 and compared with the WOA18 climatology.

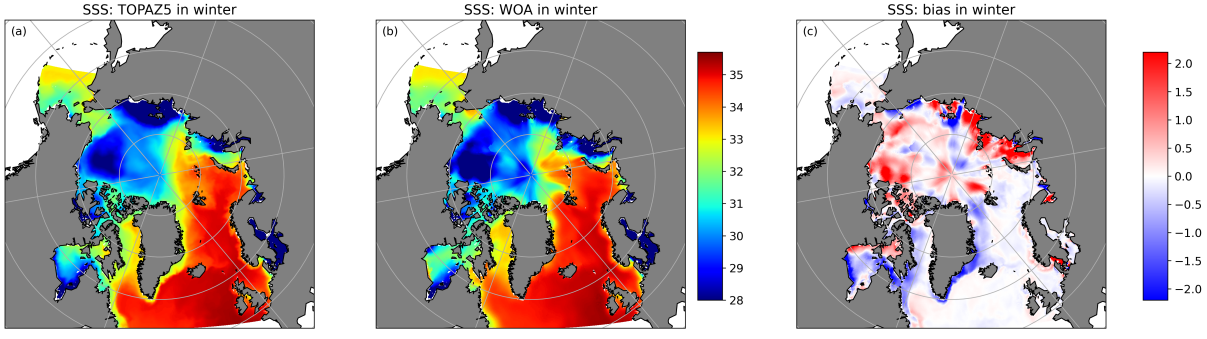

https://doi.org/10.5194/egusphere-2026-1520
Preprint. Discussion started: 8 May 2026

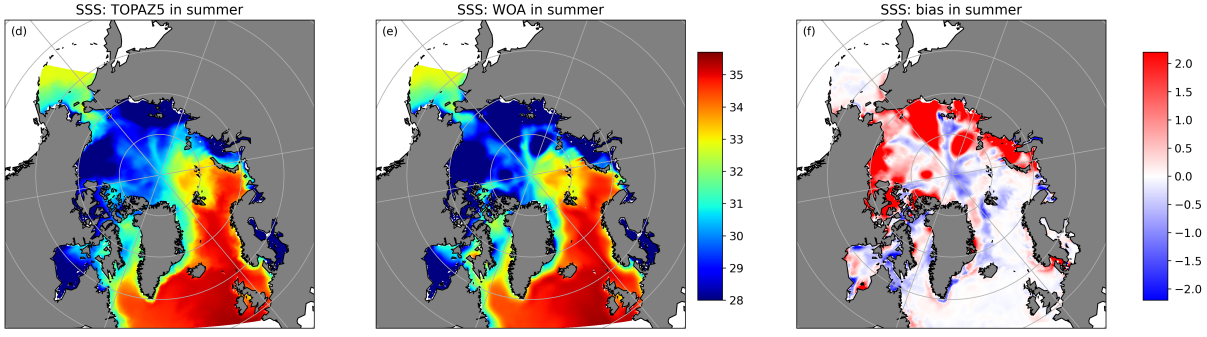

195

Fig. 3. Maps of the SSS means in winter (a, b) and summer (d, e) from TOPAZ5 and WOA, and their difference (Model - WOA) (c, f). Seasonal means are computed over January-March (winter), and July-September (summer) for 2009-2019.

The model reproduces the large-scale salinity structure in the Nordic Seas in good agreement with WOA climatology. 200 However, salinity in the Beaufort and Laptev Seas is higher in the model in both winter and summer, with differences reaching about 2 in winter and exceeding 2 in summer, particularly over the Arctic shelf regions.

Basin-averaged statistics over the ice-free domain indicate that SSS exhibits a weak freshening trend of -0.008 yr^{-1} over the analysis period. The model shows a mean bias of -0.21 relative to WOA and an RMSE of 0.24 (Table 1). Note that the salinity is a dimensionless quantity.

205

3.1.3 Seasonal cycle

The mean annual cycle of the domain-averaged SST and SSS for 2009-2019, excluding the ice-covered Arctic, is shown in Fig. 4.

https://doi.org/10.5194/egusphere-2026-1520
Preprint. Discussion started: 8 May 2026

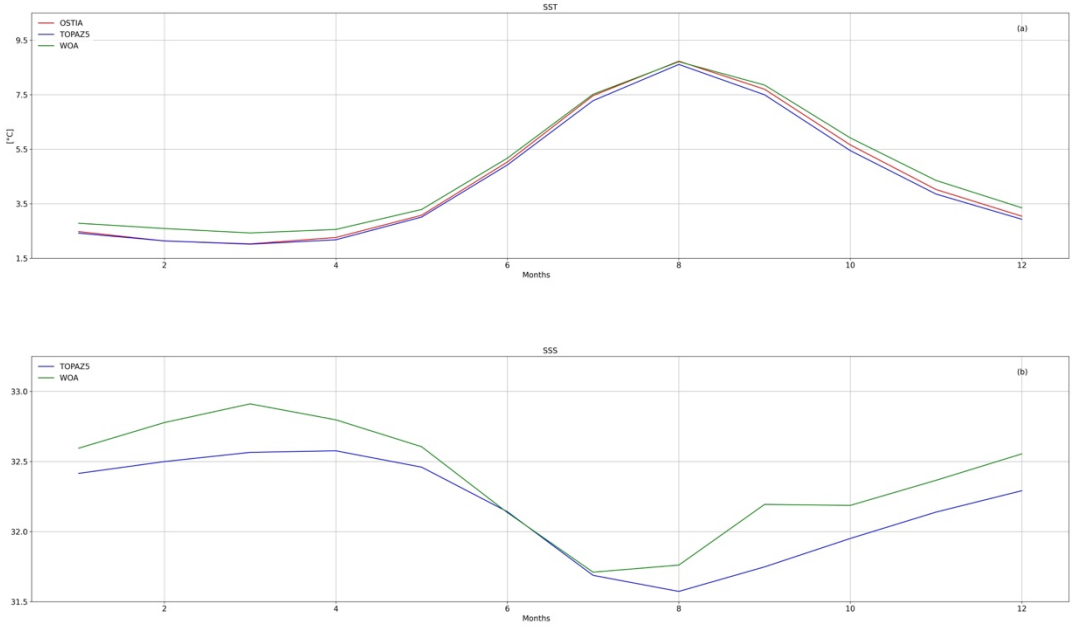

Fig. 4. Mean annual cycle of domain-averaged (a) SST (°C) and (b) SSS for 2009-2019, excluding the Arctic region. SST: TOPAZ5 (blue), OSTIA (red), WOA (green); SSS: TOPAZ5 (blue), WOA (green).

TOPAZ5, OSTIA, and WOA climatology follow a similar seasonal cycle in SST (Fig. 4a), with maximum values in August (approximately 8.5 - 9 °C) and minima in February-March (around 2 °C). TOPAZ5 and OSTIA are in close agreement throughout the year in both phase and magnitude. WOA is generally slightly warmer than both TOPAZ5 and OSTIA, particularly during summer and early autumn. Consequently, differences between TOPAZ5 and OSTIA remain small across all months, while TOPAZ5 is slightly cooler than WOA, with the largest deviations occurring during the warm season.

The domain-averaged SSS (Fig. 4b) from TOPAZ5 and WOA also shows a consistent seasonal cycle, with salinity peaking in late winter to early spring (March-April) and reaching a minimum in late summer (around August). TOPAZ5 is consistently fresher than WOA throughout most of the year. The differences are smallest during winter and increase toward late summer and early autumn, suggesting enhanced surface freshening in the model during periods of increased freshwater input. This behaviour is consistent with the overall freshening tendency (-0.008 yr^{-1}) over the analysis period (Table 1).

Note that the time series and trends are computed over the ice-free domain, whereas spatial maps include Arctic regions where the model exhibits positive salinity biases, particularly over the Beaufort and Laptev shelves. This explains why basin-averaged SSS statistics show a negative bias, whereas spatial maps reveal strong positive biases in Arctic shelf regions.

https://doi.org/10.5194/egusphere-2026-1520
Preprint. Discussion started: 8 May 2026

3.2 Vertical hydrographic structure along key sections

The model hydrography was evaluated against observations along three hydrographic sections (Fig. 1): Svinøy in the Norwegian Basin, Gimsøy in the Lofoten Basin, and the Barents Sea Opening (BSO) at the entrance to the Barents Sea. Monthly mean values for March and August, averaged over 2009-2019, were used to represent winter and summer conditions. The Gimsøy section is shown in the main manuscript, while the Svinøy and BSO sections are provided in Appendices A and B. All three sections are described in detail in the text.

3.2.1 Gimsøy section

In March (Fig. 5), temperature and salinity distributions reveal two distinct regions. The eastern section is dominated by relatively cold and fresh coastal water, with temperatures between 5 and 5.5 °C and salinities below 34, a feature captured by both observations and TOPAZ5. The central and western regions are characterised by Atlantic Water, with surface temperatures up to 6.5 °C and salinities exceeding 35.

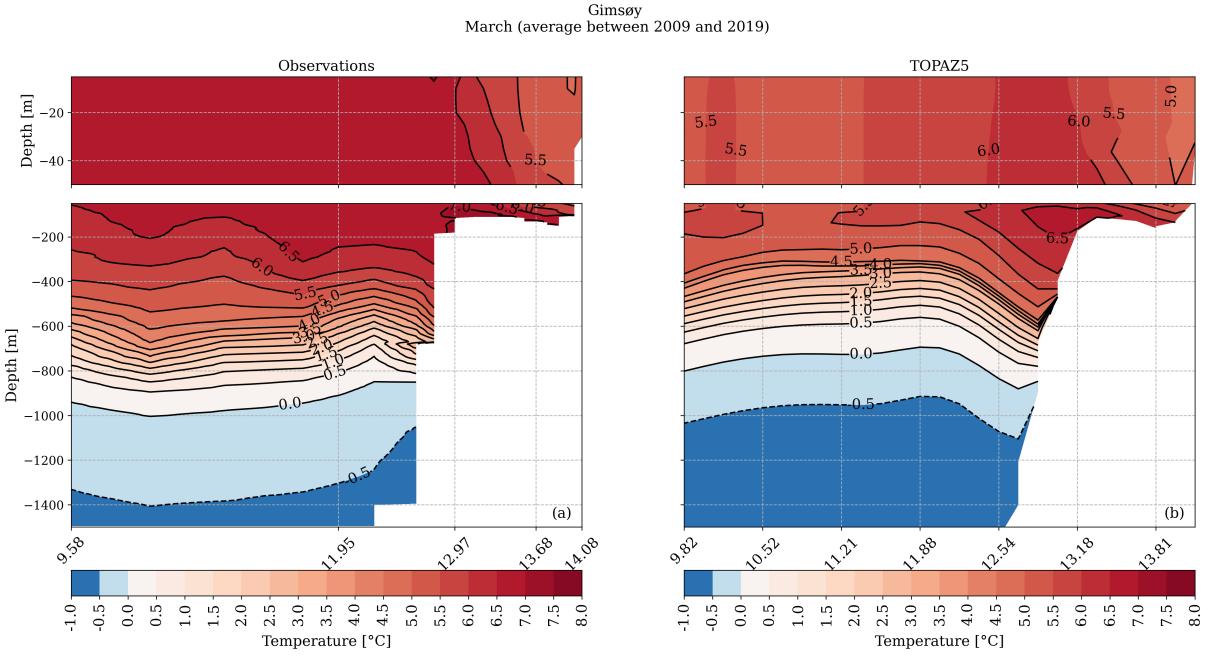

https://doi.org/10.5194/egusphere-2026-1520
Preprint. Discussion started: 8 May 2026

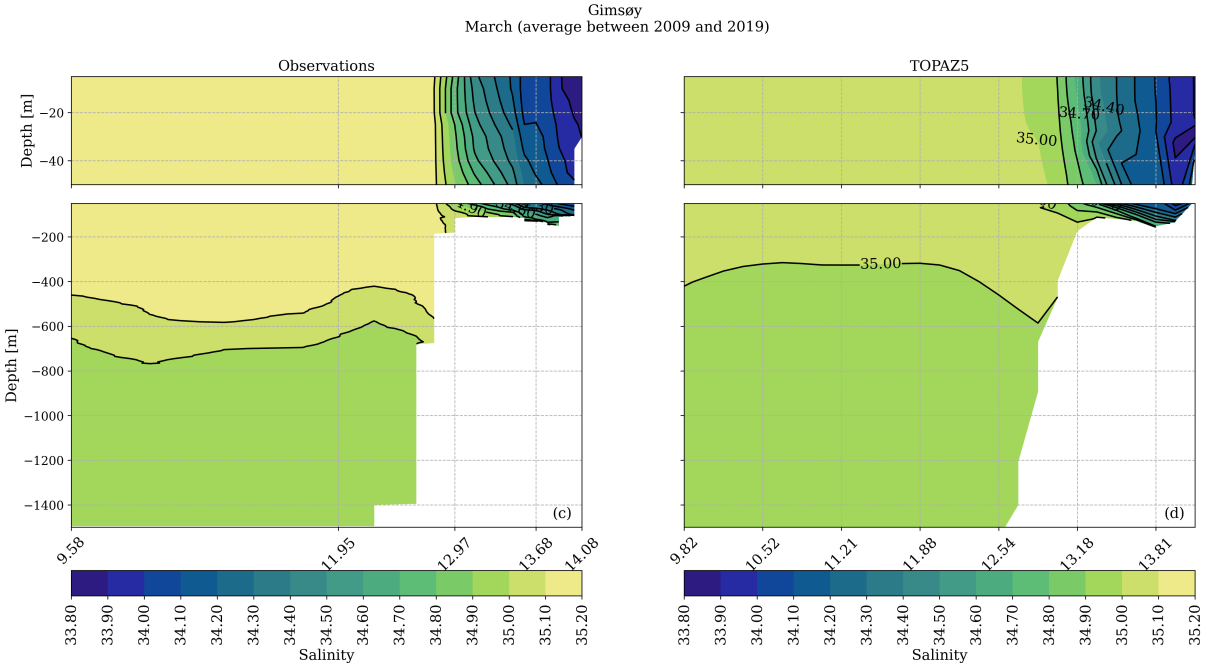

Fig. 5. Vertical cross section at the Gimsøy section showing mean March temperature (°C; panels a and b) and salinity (panels c and d) from observations (left) and TOPAZ5 (right), averaged over the period 2009-2019.

In August (Fig. 6), stratification intensifies. Observed surface temperatures range from 8 to 13.5 °C, with a distinct thermocline between 50 and 200 m depth, separating warm surface waters from colder waters (~1 °C) below. This vertical structure is accompanied by a rapid salinity transition, from fresher surface waters (salinity ~34) to uniform saline layers (~35) below 200 m. TOPAZ5 captures the thermocline and deep-water properties but overestimates surface temperature and salinity during summer.

https://doi.org/10.5194/egusphere-2026-1520
Preprint. Discussion started: 8 May 2026

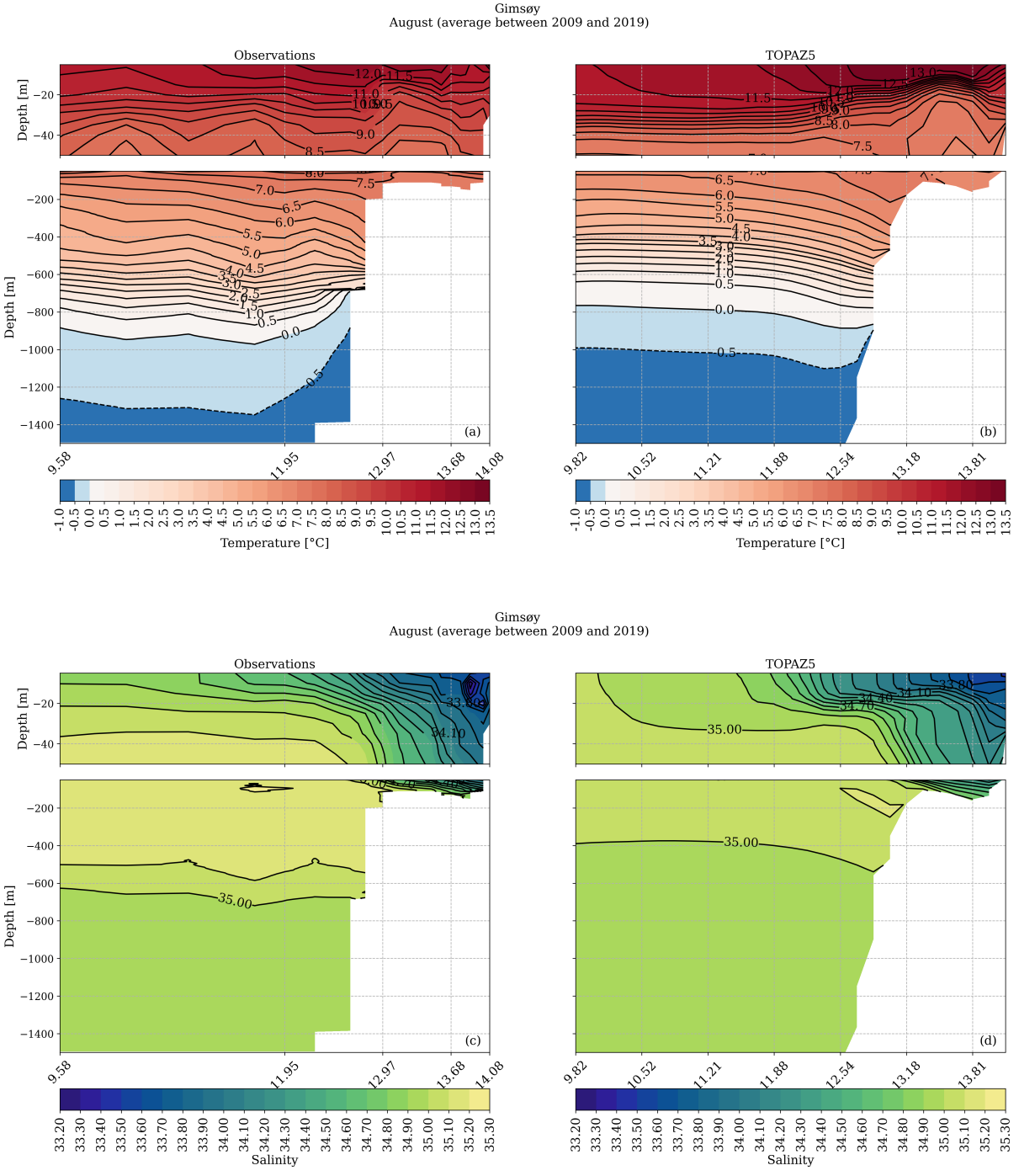

Fig. 6. Same as Fig. 5, but for August.

https://doi.org/10.5194/egusphere-2026-1520
Preprint. Discussion started: 8 May 2026

3.2.2 Svinøy section

At the Svinøy section, overall temperatures are higher than at the Gimsøy and BSO sections, consistent with it being further south and located near the core of the Norwegian Atlantic Current. In March (Fig. A1), the water column is cooler, with the 5 °C isotherm reaching depths of approximately 500 m, indicating deeper stratification compared to other seasons. In August (Fig. A2), observed surface temperatures exceed 14 °C, with a well-defined thermocline between 100 and 200 m depth.

Salinity observations indicate the predominance of AW, with values between 34.8 and 35.0 throughout the column and limited surface freshening, reflecting minimal Arctic freshwater influence. TOPAZ5 captures the general structure of both temperature and salinity but systematically underestimates surface temperatures and overestimates vertical mixing at intermediate depths, resulting in smoother thermocline and halocline structures than observed.

3.2.3 BSO section

The BSO section exhibits marked seasonal variability between winter (Fig. B1) and summer (Fig. B2) in both temperature and salinity. In March, observed temperatures are relatively homogeneous in the upper 200 m, with values ranging between 4 °C and 6 °C, indicative of well-mixed conditions during winter. Below 200 m, temperatures decrease gradually, reaching 2-3 °C near the bottom. The August means show pronounced stratification. Surface temperatures reach approximately 11-12 °C due to summer heating, while colder waters (~2-3 °C) dominate below 300 m. In this region, TOPAZ5 slightly underestimates summer surface warming and tends to smooth the thermocline gradient. In terms of salinity, March observations demonstrate uniformity (~34.5) in the upper 200 m, reflecting deep winter mixing and limited freshwater influence. Below this depth, salinity increases slightly with depth. In August, surface freshening is apparent, with salinities decreasing to ~34, driven by enhanced freshwater inputs and seasonal stratification. A pronounced halocline separates the fresher surface layer from the saltier, deeper layers. TOPAZ5 reasonably captures the deeper salinity structure but consistently overestimates surface salinities in both seasons. This bias is particularly notable in August, when the model underestimates the surface freshening and smooths the halocline gradient as it does for the thermocline. These regional differences reflect varying model performance across the inflow branches of Atlantic Water.

3.3 SLA

In this paper, the SLA is defined as the deviation of the monthly SSH from the mean SSH estimated over the 2009-2019 period. Spatial distribution maps of SLA trends (mm yr^{-1}) during this period, derived from TOPAZ5, satellite altimetry, and GLORYS (Fig. 7), reveal significant regional variability in sea level changes.

The altimetry-derived SLA trends exhibit the most extensive spatial coverage and highest magnitudes of positive trends among the datasets, reaching local maxima of 10 mm yr^{-1}. Pronounced positive trends dominate the Barents Sea and Nordic

https://doi.org/10.5194/egusphere-2026-1520
Preprint. Discussion started: 8 May 2026

290 Seas, while negative trends are concentrated in the southwestern domain, encompassing the Labrador Sea and North Atlantic Subpolar Gyre.

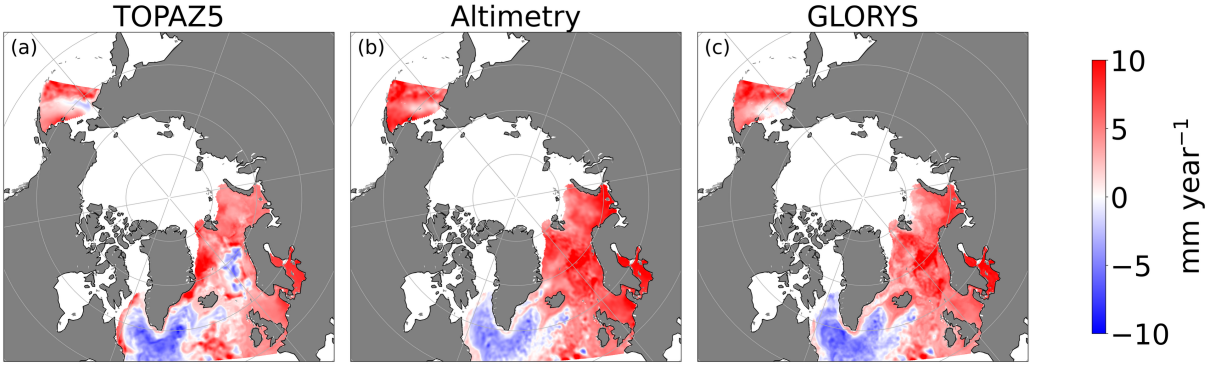

Fig. 7. SLA trends (mm yr^{-1}) for the period 2009-2019 for TOPAZ5 (a), Altimetry (b) and GLORYS (c).

295

The SLA trends from GLORYS reproduce the large-scale altimetry pattern with high fidelity, but exhibit less detailed spatial variability, likely due to smoothing in the reanalysis product. It captures the positive trends in the Nordic Seas and northeastern Atlantic, and the negative trends in the southwestern domain (Labrador Sea and North Atlantic Subpolar Gyre).

TOPAZ5 replicates the large-scale SLA trends structure observed in both reference datasets (altimetry and GLORYS). It 300 shows positive trends along the Pacific boundary, throughout the North Atlantic, and in the Barents, Greenland, and Norwegian Seas. The Barents Sea exhibits particularly strong inter-dataset agreement with consistently positive trends. TOPAZ5 also simulates the extensive negative trends in the southwestern domain, aligning closely with altimetry and GLORYS in the Labrador Sea and North Atlantic Subpolar Gyre. The primary deviation occurs in the Norwegian Sea (specifically the Lofoten and Norwegian Basins), where TOPAZ5 displays localized trends heterogeneity, potentially 305 reflecting steric-driven variability or circulation changes, in contrast to the more spatially coherent positive trends seen in the altimetry data.

Despite regional differences, all three datasets consistently show positive SLA trends in the AW inflow regions (Fram Strait and Greenland Sea) and negative trends in the southern domain, reflecting robust large-scale processes (e.g. AW inflow and freshwater accumulation). However, TOPAZ5 exhibits significant discrepancies, most notably a substantial underestimation 310 of the positive trends magnitude within the critical AW accumulation area of the Lofoten Basin compared to altimetry and GLORYS. TOPAZ5 also underestimates positive trends in the Barents and Greenland Seas relative to both observations and GLORYS. The temporal evolution of SLA, averaged over the altimetry domain from 2009 to 2019, provides further insights into the dynamics of sea level rise (Fig. 8).

https://doi.org/10.5194/egusphere-2026-1520
Preprint. Discussion started: 8 May 2026

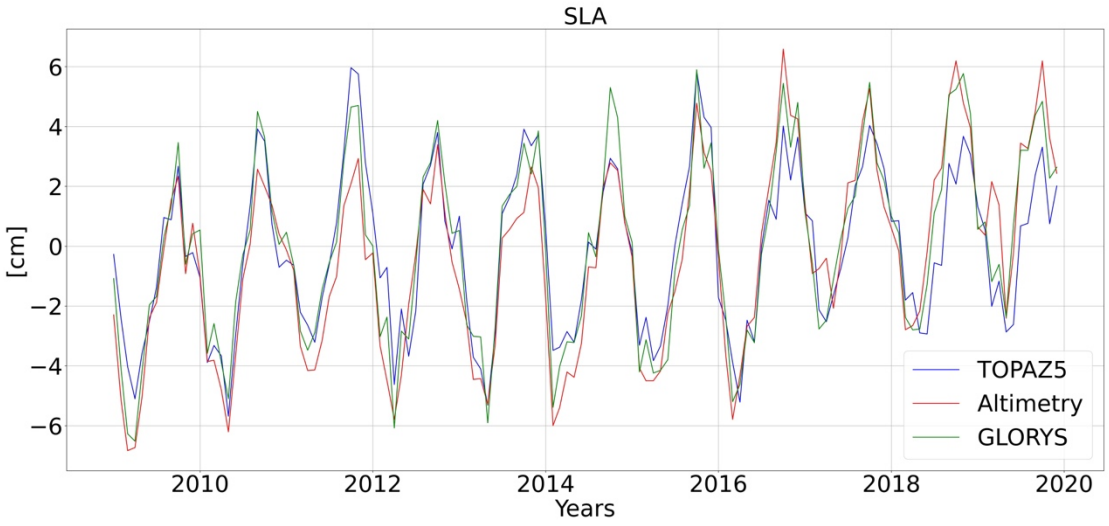

Fig. 8. Time series of the sea level anomaly (SLA) monthly means over the Altimetry domain for the period 2009-2019 for TOPAZ5 (blue), Altimetry (red) and GLORYS (green).

Time series from TOPAZ5 and GLORYS show similar trends, maintaining a consistent difference throughout the analysis period (Fig. 8). However, the altimetry data reveal a continued rise in SLA starting in 2016, while the models begin to show a decrease, indicating a divergence between observed and modelled SLA. In addition, differences in peak amplitude are evident, with altimetry recording higher values, suggesting limitations in the resolution of TOPAZ5. These shortcomings, particularly in representing AW retention dynamics, may also be related to the absence of data assimilation, highlighting specific targets for further investigation and model refinement.

3.4 EKE

We assess the SSH variability as a proxy for EKE (Section 2.2) using satellite altimetry and GLORYS as references (Fig. 9).

https://doi.org/10.5194/egusphere-2026-1520
Preprint. Discussion started: 8 May 2026

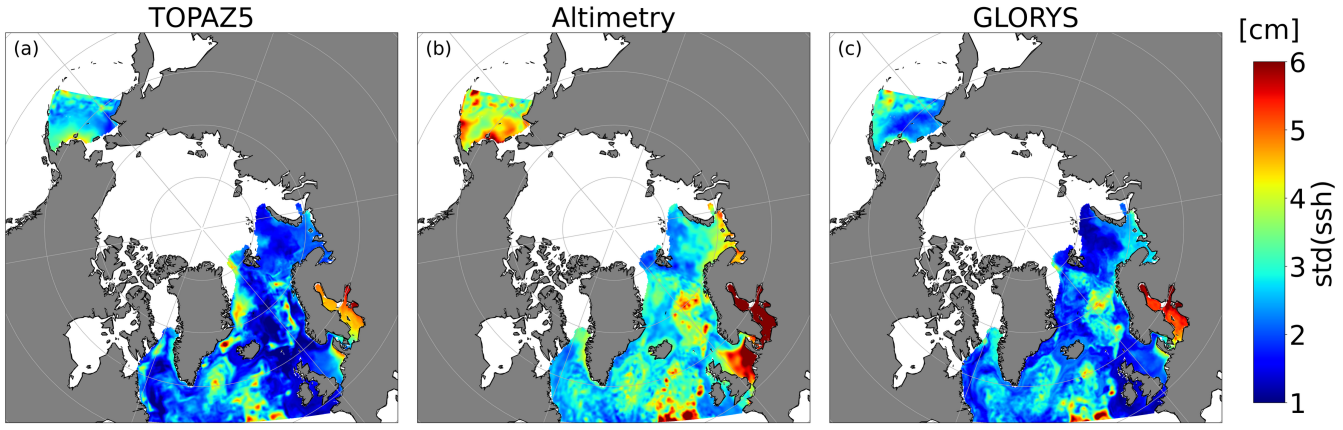

Fig. 9. Standard deviation of SSH (EKE proxy) over the period 2009-2019 for TOPAZ5 (a), Altimetry (b) and GLORYS (c).

TOPAZ5 successfully captures the large-scale spatial distribution of mesoscale variability across the North Atlantic and Arctic Ocean. TOPAZ5 shows a band of elevated SSH variability along the Atlantic inflow pathway between Svalbard and the Greenland Sea with major eddy-active zones in the western North Atlantic, Labrador Sea, and along continental slopes. However, TOPAZ5 consistently underestimates the amplitude of SSH variability compared to altimetry observations and, to a lesser extent, GLORYS. This underestimation is pronounced in several key regions: the Barents Sea (where altimetry shows standard deviations up to ~4 cm), the Gulf Stream and North Atlantic Current systems, the Labrador Sea, and across the Greenland and Norwegian Seas. Within the Nordic Seas, the deficit is particularly acute in the Lofoten Basin, the region's most eddy-active area, where TOPAZ5 fails to simulate the semi-permanent Lofoten Eddy, a key modulator of regional EKE (Raj et al., 2015; Søiland et al., 2016; Drinkwater et al., 2020). Deficiencies also extend to other topographically complex regions (Vøring Plateau, Mohn Ridge), where local bathymetry strongly influences eddy generation. In shallow shelf regions like the North and Baltic Seas, both TOPAZ5 and GLORYS underestimate the high coastal variability observed by altimetry (standard deviations up to ~6 cm), with TOPAZ5 exhibiting particularly low values. These limitations, especially the systematic underestimation of EKE amplitude in dynamically active and topographically constrained regions, highlight TOPAZ5's limitations in resolving small-scale eddies. This suggests that enhanced horizontal resolution, or advanced assimilation techniques may be needed for more accurate representation of mesoscale dynamics.

3.5 MLD

The MLD in the North Atlantic has a strong seasonal cycle (de Boyer Montégut et al., 2004; Holte et al., 2017). We therefore compare summer and winter values separately for TOPAZ5 validation. The winter MLD (resp. summer) means are averaged over the months of January to March (July to September), over the time period 2009-2019 (Fig. 10).

https://doi.org/10.5194/egusphere-2026-1520
Preprint. Discussion started: 8 May 2026

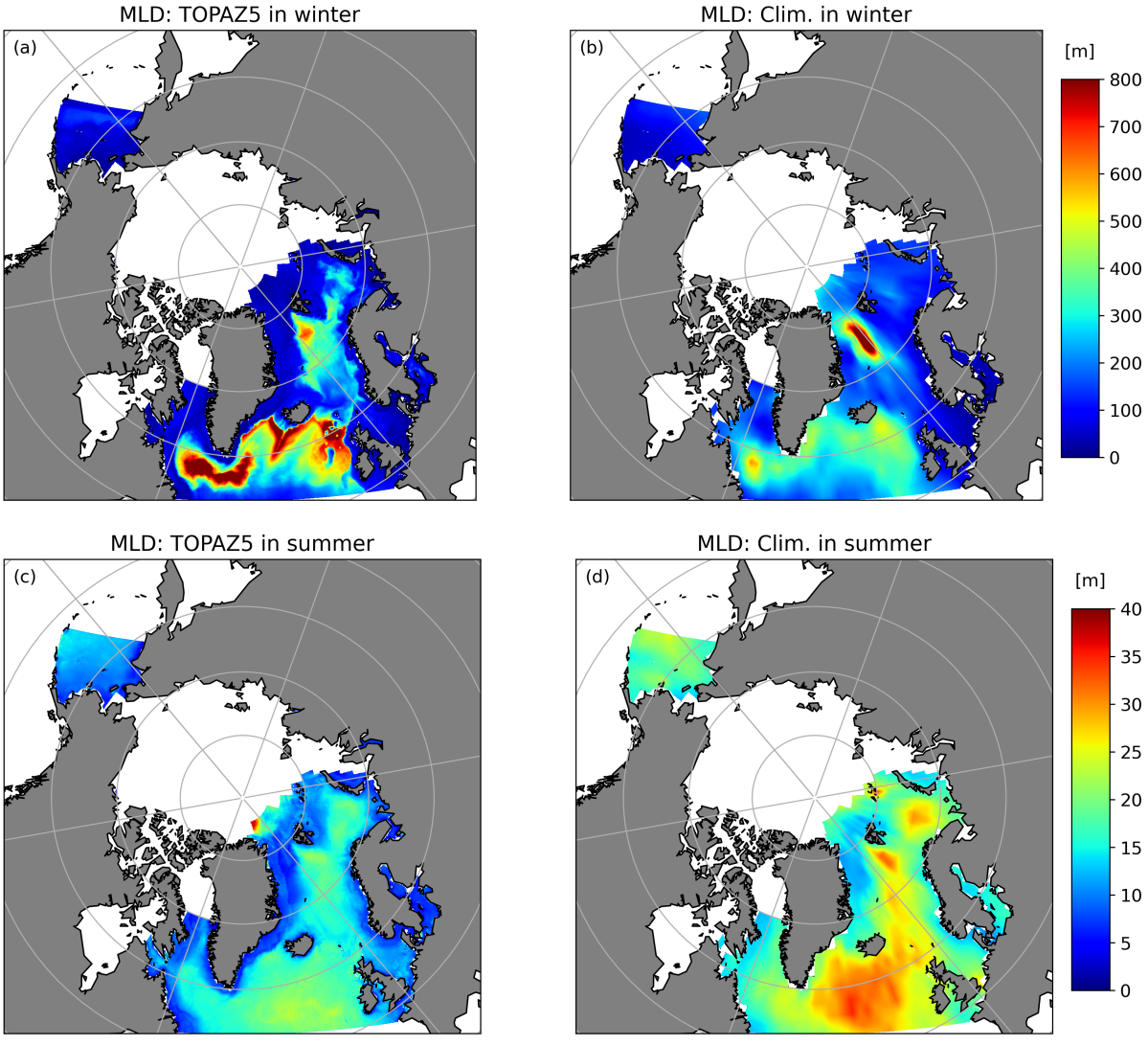

355

Fig. 10. Maps of the MLD means in winter (a, b) and summer (c, d) for TOPAZ5, and climatology. The winter (resp. summer) MLD means are computed over the months of January to March (July to September), over the period 2009-2019.

TOPAZ5 simulates deep winter MLDs (>700 m, Fig. 10a) in the Greenland Sea, Labrador Sea, and parts of the North
360 Atlantic, indicating intense convection and deep-water formation. In the Greenland and Labrador Seas, deep convection is driven primarily by strong surface cooling (Marshall and Schott, 1999; Pickart et al., 2003; Yashayaev, 2024). Across the ice-free North Atlantic, deep MLDs result mainly from surface heat loss and wind-driven mixing (de Boyer Montégut et al., 2004; Piunno et al., 2025).

https://doi.org/10.5194/egusphere-2026-1520
Preprint. Discussion started: 8 May 2026

The climatology (Fig. 10b), characterized by its smoother representation and generally lower MLD values, is affected by the limited availability of hydrological profiles in certain regions, particularly in the subpolar North Atlantic and Arctic-adjacent seas, where observational coverage is sparse (de Boyer Montégut et al., 2004). In contrast, other parts of the North Atlantic, especially at lower latitudes, are better sampled and thus less impacted by this limitation.

While spatial patterns align, climatological MLDs are generally shallower than in TOPAZ5 (except in the central Greenland Sea). This suggests that TOPAZ5 generally simulates stronger vertical mixing. The model simulates MLDs >1000 m in the Labrador Sea (driven by cooling and wind mixing), ~800 m in the Irminger Sea (driven by winter storms) and 500-600 m in Greenland Sea (where brine rejection enhances convection).

Summer MLDs (Fig. 10c and 10d) are shallower than in winter due to surface heating, reduced wind mixing, and stronger stratification of the water column. TOPAZ5 simulates summer MLDs typically <40 m, except locally near Arctic ice edges (20-30 m), slightly exceeding winter values in those areas.

3.6 Transport

We have computed the net volume transport of different water masses (hereafter referred to as transport) through selected sections (Fig. 1 and Table 2) from daily averages over the time period of 2009-2019 for TOPAZ5.

Table 2: Section names, positions and targeted waters.

Section name	Section position	Water mass targeted
Pacific boundary	(172.83; 61.84) to (-172.39; 52.02)	All waters
Bering Strait (BS)	(-169.7; 66.0) to (-167.47; 65.67)	All waters
Fram Strait (FS)	(10.0; 78.83) to (-8.0; 78.83)	AW (T > 2 ˚C)
Barents Sea Opening (BSO)	(20.0; 70.5) to (19.167; 74.25)	AW (T > 3 ˚C; S > 35)
Gimsøy	(14.07; 68.4) to (8.2; 70.4)	AW (T > 5 ˚C; S > 35)
Svinøy	(5.2; 62.367) to (0.0; 64.667)	AW (T > 5 ˚C; S > 35)
Faroe Shetland Channel (FSC)	(-3.0; 59.5) to (-6.5; 61.33)	AW (T > 5 ˚C; S > 35)
Atlantic boundary	(-0.92; 47.8) to (-57.55; 53.1)	All waters

https://doi.org/10.5194/egusphere-2026-1520
Preprint. Discussion started: 8 May 2026

The volume transports are compared to available observation-based estimates (Table 3).

Table 3: Net volume transport across the sections over the period 2009-2019. Positive values are northward, negative southward.

Section	Water mass	TOPAZ5 (Sv)	Literature (Sv)
Pacific boundary	All waters	0.83	-
BS	All waters	0.79	0.8 (Woodgate et al., 2006) 0.7 (Smedsrud et al., 2022)
FS	AW (T > 2 ˚C)	1.34	3 ± 0.2 (Beszczynska-Möller et al., 2012)
BSO	AW (T > 3 ˚C; S > 35)	1.37	2.0 ± 1.0 (Lien et al., 2016)
Gimsøy	AW (T > 5 ˚C; S > 35)	2.8	-
Svinøy	AW (T > 5 ˚C; S > 35)	3.7	4.4 ± 1.0 (Lien et al., 2016)
FSC	AW (T > 5 ˚C; S > 35)	3.3	2.7 ± 1.0 (Lien et al., 2016)
Atlantic boundary	All waters	-0.82	-

The net volume transport into the model domain is approximately 0.83 Sv (1 Sv = 10^6 m^3s^{-1}) through the northern (Pacific) boundary, balanced by an estimated 0.82 Sv outflow through the southern (Atlantic) boundary. The modelled total flux of water masses through the Bering strait for the period 2009-2019 (0.79 Sv) is comparable to the estimation of 0.8 Sv reported by Woodgate et al. (2006) for the period 1990-2004.

For the sections intersecting the North Atlantic Current, the FSC, Svinøy and BSO, we compared the modelled volume transport of AW from TOPAZ5 with observational estimates from Lien et al. (2016) for the period 1997-2009. TOPAZ5 slightly overestimates the mean AW transport through the FSC (3.3 Sv) compared to the observed value of 2.7 ± 1.0 Sv. Conversely, the mean transport through the Svinøy section is somewhat underestimated in the model (3.7 Sv) relative to observations (4.4 ± 1.0 Sv). It should be noted that the Svinøy section in this study extends further west than the one in Lien et al. (2016) who reports a total northward transport of 6.2 Sv, composed of 2.7 Sv through the FSC and 3.5 Sv through the Faroe North (FN) section, our estimate is based on transport calculated across the entire Svinøy section. Our computation yields a total northward transport of 3.7 Sv through the Svinøy line, which inherently includes contributions from both the FSC and FN pathways. By integrating across the full Svinøy section, we account for all northward-flowing waters entering the Nordic Seas, including those passing north of the Faroe Islands. As such, our estimate can be considered comprehensive, whereas Lien's estimate is a composite sum of distinct sub-sections.

https://doi.org/10.5194/egusphere-2026-1520
Preprint. Discussion started: 8 May 2026

For the BSO, TOPAZ5 simulates 1.37 Sv, slightly below the observed 2.0 ± 1.0 Sv. Although the modelled means differ somewhat from the observational central values, all simulated transports fall within the observational uncertainty ranges. The reduced volume transport toward the BSO may suggest a weakening of the AW inflow into the Arctic in the model, although further analysis, such as direct computation of heat transport, would be needed to determine whether this volume transport reduction corresponds to a significant change in AW heat delivery to the Arctic.

In the FS section, we adopted the definition of AW used by Beszczynska-Möller et al. (2012), identifying waters warmer than 2 °C. Beszczynska-Möller et al. (2012) estimated the volume transport through FS to be 3.0 ± 0.2 Sv for the period 1997-2010. In contrast, TOPAZ5 estimates for the same period were lower at 1.22 Sv. For the analysis period of this study (2009-2019), TOPAZ5 estimates a similar AW transport of 1.34 Sv through FS.

3.7 Sea Ice

The spatial distribution of sea ice thickness simulated by TOPAZ5 exhibits broadly consistent large-scale patterns when validated against CS2SMOS observations across the Arctic, as shown in March (Fig. 11).

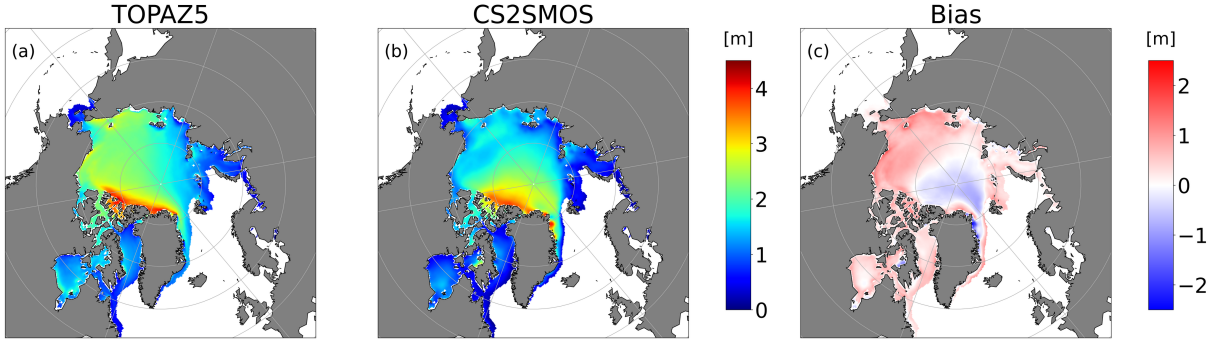

Fig. 11. Sea ice thickness in March over the period 2011-2019 from TOPAZ5 (a), CS2SMOS (b), and their bias (c).

The model successfully reproduces the observed concentration of thick multi-year ice (>4 m) north of the Canadian Arctic Archipelago and Greenland, regions characterized by the oldest and most compacted sea ice. In contrast, both TOPAZ5 and CS2SMOS show significantly thinner ice (<1 m) in the MIZ, including the Barents Sea, Bering Sea, and along the Siberian Arctic coast, where warmer ocean waters and elevated melt rates prevail. Furthermore, TOPAZ5 accurately captures the pronounced gradient in sea ice thickness from the central Arctic basin toward these peripheral regions, indicating that key large-scale dynamic processes, such as ice advection and divergence, are well represented in TOPAZ5.

Despite general agreement at the basin scale, several regional discrepancies between TOPAZ5 and observations are evident. The model tends to overestimate sea ice thickness across much of the central and western Arctic, with positive biases reaching up to 2 meters, especially north of Greenland and the Canadian Arctic Archipelago (Fig. 11c). These

https://doi.org/10.5194/egusphere-2026-1520
Preprint. Discussion started: 8 May 2026

overestimations may be partly attributed to observational uncertainties, such as radar signal penetration depth and algorithmic assumptions in CS2SMOS retrievals, but also likely reflect biases inherent in the model's physical parameterizations. Similarly, TOPAZ5 overestimates the sea ice thickness by up to 2 meters along the Siberian Arctic coast, a region characterized by rapid and complex ice-ocean interactions. Additional regional mismatches are observed off eastern Greenland, near Svalbard, and in the Beaufort and East Siberian Seas. In the Beaufort Sea, the model simulates enhanced ice convergence, likely driven by the EVP rheology, which has been shown to overestimate drift under wind and ocean forcing (Sakov et al., 2012; Johnson et al., 2012). In the Siberian Sea, this locally thicker ice compared to observations points to an overestimation of wind-driven ice transport in the region.

Comparisons between seasonal sea ice concentration (Fig. 12) further support the model's ability to reproduce observed patterns, although with varying levels of accuracy.

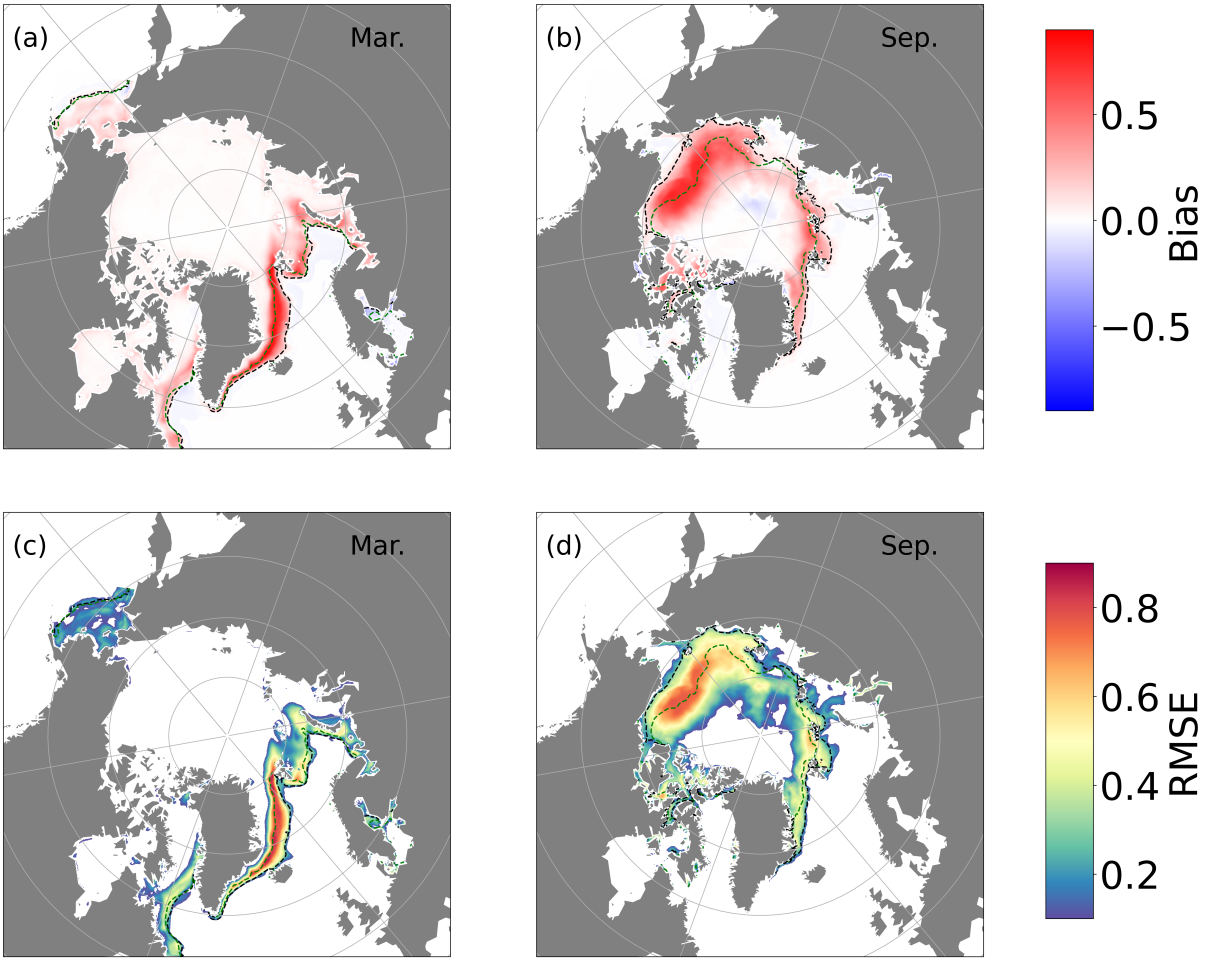

Fig. 12. Spatial bias (a, b) and RMSE (c, d) of sea ice concentration in TOPAZ5 compared to OSI-SAF for March (left) and September (right), calculated from monthly averages for the period 2009-2019. Dashed lines show the 15% sea ice edge in TOPAZ5 (black) and OSI-SAF (green). RMSE values below 0.1 are masked.

https://doi.org/10.5194/egusphere-2026-1520
Preprint. Discussion started: 8 May 2026

In March, during maximum ice extent, RMSE values increase substantially along the MIZ, reaching 0.4 - 0.8 in areas such as the Bering, Labrador, and Barents Seas (Fig. 12c). In September, when sea ice extent reaches its minimum, RMSE values are over a large region, particularly in the Beaufort, Chukchi, and Siberian Seas (Fig. 12d). These elevated errors highlight the model's difficulty in representing thinner and more fragmented ice during late summer, although agreement in the central Arctic remains comparatively robust.

Overall, spatial patterns of RMSE and ice thickness bias reveal that model-observation discrepancies are highly dependent on both season and region. TOPAZ5 performance is generally strongest in the central Arctic, where the sea ice is thicker and more stable, and weakest along dynamic marginal zones, especially during the melt season. High RMSE values are simulated along the MIZ in March. In September, model errors are further amplified by the complex evolution of melt ponds and surface heat fluxes under retreating ice conditions.

4 Discussion

This study evaluates the performance of TOPAZ5 in simulating key physical processes in the North Atlantic and Arctic. Overall, TOPAZ5 shows strong skill in capturing large-scale hydrographic structures, mixed layer depths, and the seasonal cycle of sea ice extent. However, limitations emerge in representing mesoscale dynamics, vertical stratification, and MIZ processes. These strengths and limitations highlight specific areas where improvements in resolution, parameterizations, and data assimilation, are most needed to enhance TOPAZ5 realism.

4.1 Large-scale ocean hydrography and circulation

TOPAZ5 effectively captures the pan-Arctic and North Atlantic hydrographic structure, including the northward AW transport and PW return flow. Simulated temperature, salinity, and stratification align with observed (Lien et al., 2016; Drinkwater et al., 2020) patterns and climatologies (WOA), while volume transports at key locations (Svinøy section) confirm a robust large-scale mass balance. However, persistent biases in Arctic exchanges persist, characterized by underestimated outflows through the FS and BSO and overestimated AW inflows through the FSC. These errors point to unresolved dynamics, narrow boundary currents, bathymetric steering, and AW-PW interactions, that distort Arctic freshwater and heat budgets. Refining these transports will require higher-resolution grids and improved bathymetric representations.

4.2 Vertical structure, stratification, and convection

TOPAZ5 realistically simulates deep convection (>700 m MLD) in the Labrador, Irminger, and Greenland Seas, supporting credible AMOC dynamics driven by surface heat loss and wind forcing. However, two key vertical limitations arise: (1) the

https://doi.org/10.5194/egusphere-2026-1520
Preprint. Discussion started: 8 May 2026

MLD is overestimated in the central Greenland Sea due to overly diffusive mixing schemes (de Boyer Montégut et al., 2004), and (2) weak thermocline/halocline gradients reduce vertical stratification, particularly during melt seasons. While brine rejection minimally impacts the central-basin convection, its underrepresentation, along with meltwater redistribution, exacerbates downstream hydrographic biases (Smedsrud et al., 2011). Addressing these issues demands recalibrated vertical mixing parameterizations and better freshwater flux constraints.

4.3 Regional sea surface biases

Surface properties reveal spatially coherent errors. In the Norwegian Sea, TOPAZ5 overestimates summer SST, underestimates winter SST, and exhibits persistently high melt-season SSS. These biases, coupled with weak stratification, point to challenges in the representation of vertical mixing or surface freshwater inputs rather than direct sea-ice feedback. Critically, these upstream errors propagate downstream, where unresolved Arctic processes (brine rejection, meltwater routing; Merryfield et al., 2013) amplify hydrographic inaccuracies. Improving regional fidelity hinges on better freshwater source representation and turbulence scheme refinements.

4.4 Mesoscale dynamics and sea level variability

While basin-scale SLA variability and EKE patterns are broadly captured in TOPAZ5, amplitudes are underestimated in high-energy regions (Lofoten Basin, Fram Strait, Barents Sea). The resulting smooth SLA and EKE fields highlight a trade-off between large-scale stability and fine-scale fidelity. This weakness manifests when compared to GLORYS eddy-resolving and data assimilative reanalysis (GLORYS 12 V1). Furthermore, TOPAZ5's sea-level rise (2.66 mm yr^{-1}) falls below observed trends (3.27 mm yr^{-1}; Drévillon et al., 2023), suggesting underrepresentation of thermal expansion and boundary freshwater fluxes. Enhancing mesoscale realism requires finer grids, advanced eddy parameterizations, and assimilation of SLA/surface currents.

4.5 Sea ice performance

TOPAZ5 robustly simulates the central Arctic seasonal ice cycle but struggles in the MIZ. During summer, it underrepresents the ice heterogeneity and thickness in the Beaufort and Chukchi Seas, yielding elevated errors at seasonal extremes. These shortcomings stem from inadequate physics (thin-ice dynamics) compounded by sparse observational constraints (Notz and Stroeve, 2018; Perovich et al., 2021). The MIZ accuracy will benefit from advanced rheologies and assimilation of high-resolution remote sensing data.

https://doi.org/10.5194/egusphere-2026-1520
Preprint. Discussion started: 8 May 2026

4.6 Synthesis and pathways for improvement

TOPAZ5 demonstrates proficiency in simulating large-scale North Atlantic-Arctic ocean-ice-atmosphere interactions, including AMOC-relevant convection, volume transports, and hydrography. Its core limitations, coarse resolution, simplified vertical physics, and absent data assimilation, hinder realism in:

- Mesoscale eddies and boundary currents,
- Vertical stratification and freshwater-driven processes,
- MIZ dynamics,
- High-latitude transports.

Prioritized development pathways include:

1. Increased horizontal resolution to resolve boundary currents and eddies,
2. Advanced parameterizations for vertical mixing, sub mesoscales, and ice rheology,
3. Assimilation of observations (SLA, surface currents, ice thickness) to constrain biases,
4. Improved boundary conditions, especially freshwater fluxes and sea-level forcing.

5 Conclusion

This study evaluated TOPAZ5 coupled ocean-sea ice model performance in simulating physical conditions in the North Atlantic and Arctic Ocean over 2009-2019. TOPAZ5 realistically captures large-scale ocean circulation, sea ice variability, and key seasonal hydrographic patterns, reproducing observed trends including surface warming, upper-ocean freshening, and changes in volume transport and circulation. These results highlight the model's utility for investigating climate-driven regional changes.

Persistent biases, such as warm and saline surface anomalies, underestimation of mesoscale eddy activity, and excessive central Arctic ice thickness, remain. These biases may affect the accuracy of forecasts and reanalysis, particularly in the MIZ processes and interannual variability. Targeted improvements, such as refined physical parameterizations, enhanced horizontal resolution, and advanced data assimilation, are recommended to address these issues and improve the model's fidelity.

Building on its evaluation, TOPAZ5 has been successfully implemented in the operational ocean forecasting system at the Norwegian Meteorological Institute (met.no) since January 2024. The system provides daily 10-day forecasts of ocean and sea ice conditions, with outputs publicly available via the Copernicus Marine Service portal (https://data.marine.copernicus.eu/product/ARCTIC_ANALYSISFORECAST_PHY_002_001/description).

Continued model development and validation are essential to advance understanding and improve predictive capability of Arctic and North Atlantic climate variability in a warming climate.

https://doi.org/10.5194/egusphere-2026-1520
Preprint. Discussion started: 8 May 2026

530 **Appendices**

Appendix A. Comparison of temperature and salinity at the Svinøy section

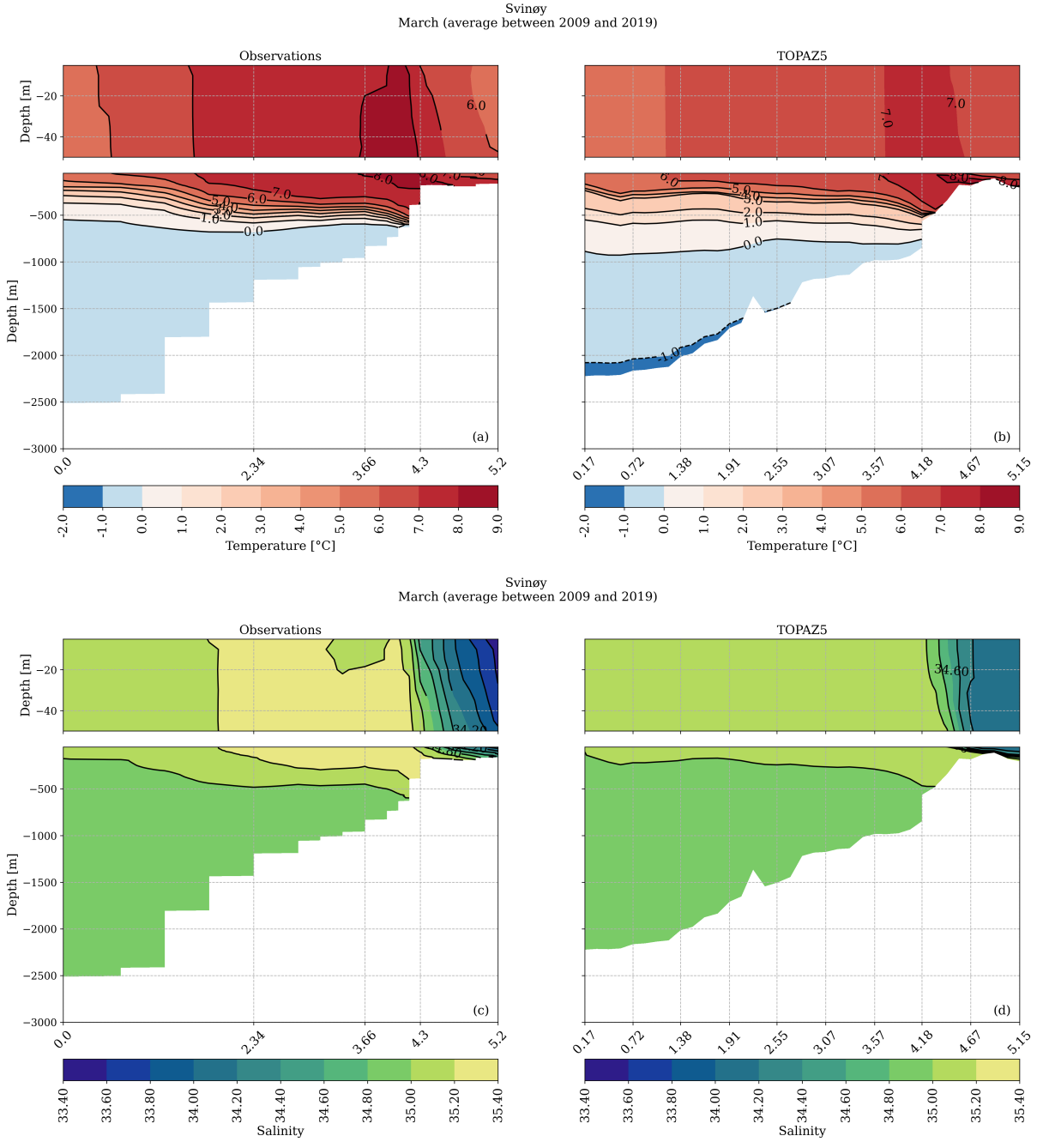

https://doi.org/10.5194/egusphere-2026-1520
Preprint. Discussion started: 8 May 2026

Fig. A1. Vertical cross section at the Svinøy section showing mean March temperature (°C; panels a and b) and salinity (panels c and d) from observations (left) and TOPAZ5 (right), averaged over the period 2009-2019.

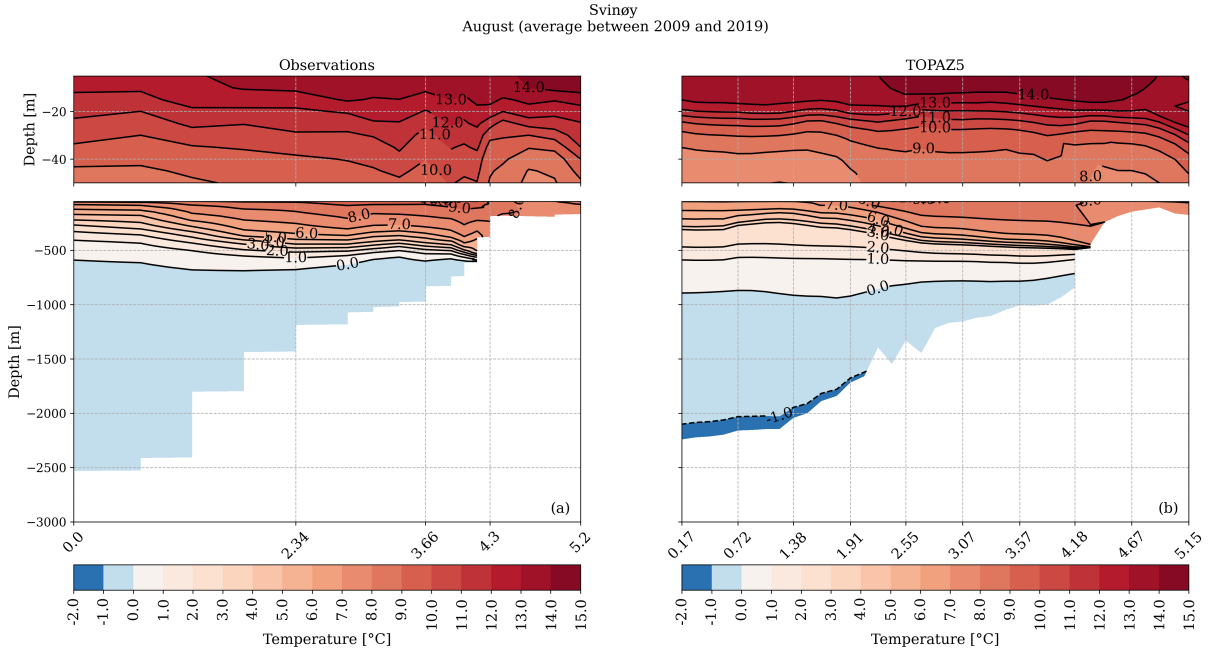

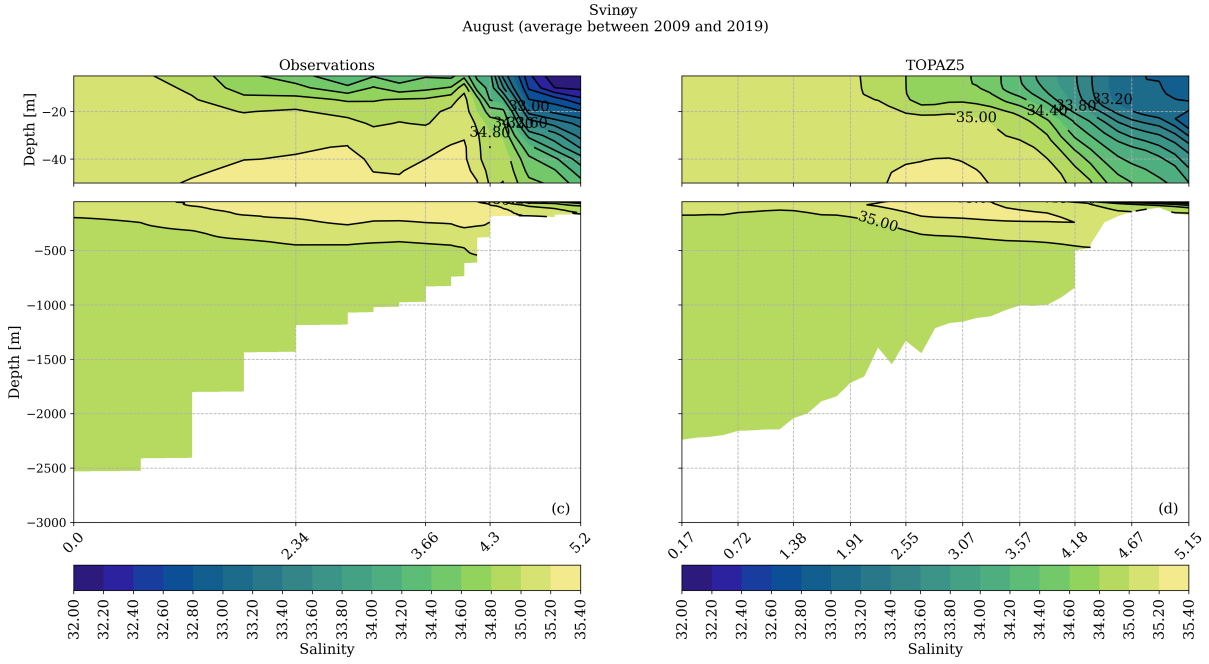

Fig. A2. Same as Fig. A1, but for August.

https://doi.org/10.5194/egusphere-2026-1520
Preprint. Discussion started: 8 May 2026

Appendix B. Comparison of temperature and salinity at the BSO section

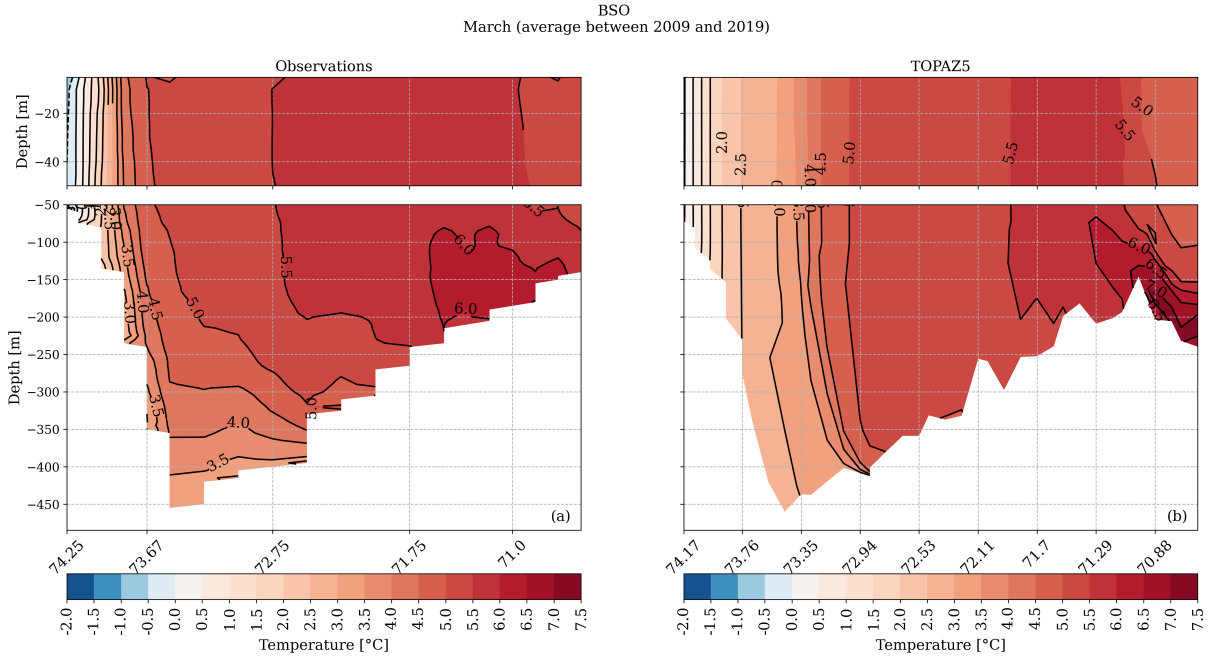

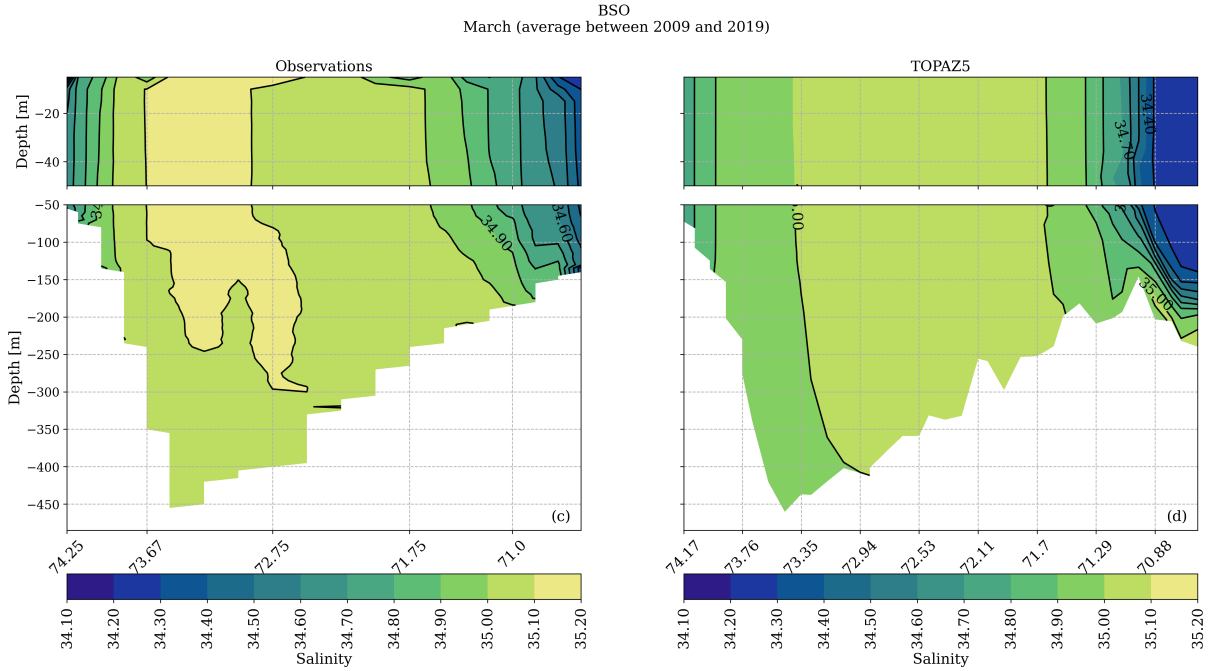

https://doi.org/10.5194/egusphere-2026-1520
Preprint. Discussion started: 8 May 2026

Fig. B1. Vertical cross section at the BSO section showing mean March temperature (°C; panels a and b) and salinity (panels c and d) from observations (left) and TOPAZ5 (right), averaged over the period 2009-2019.

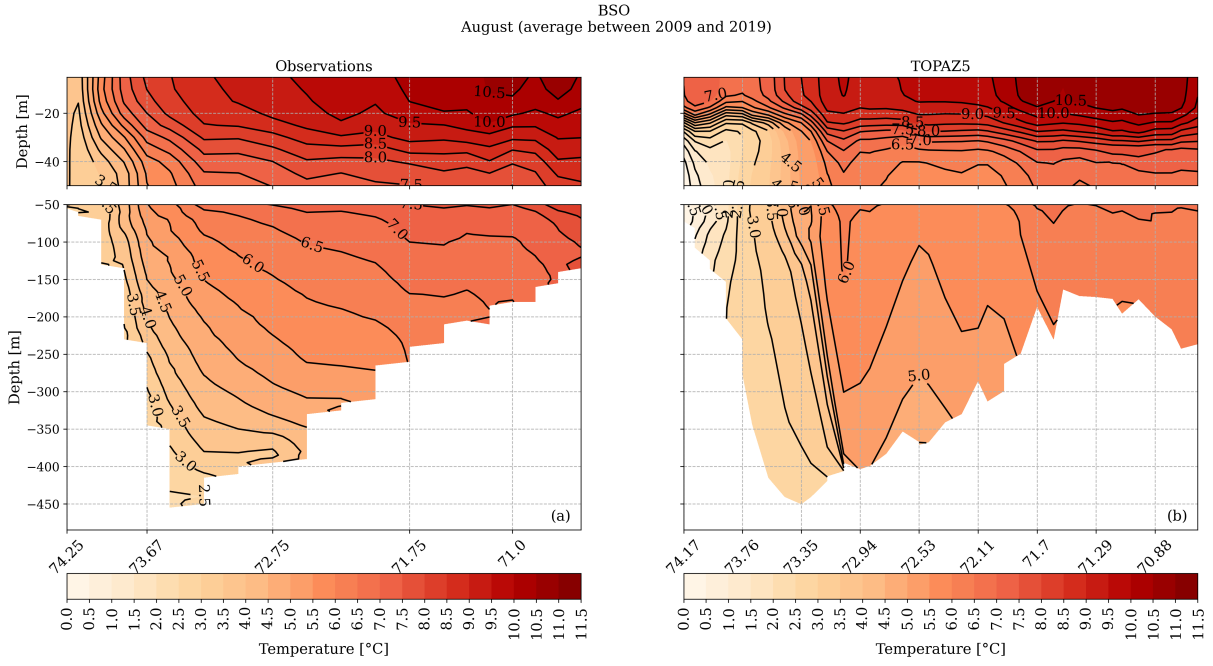

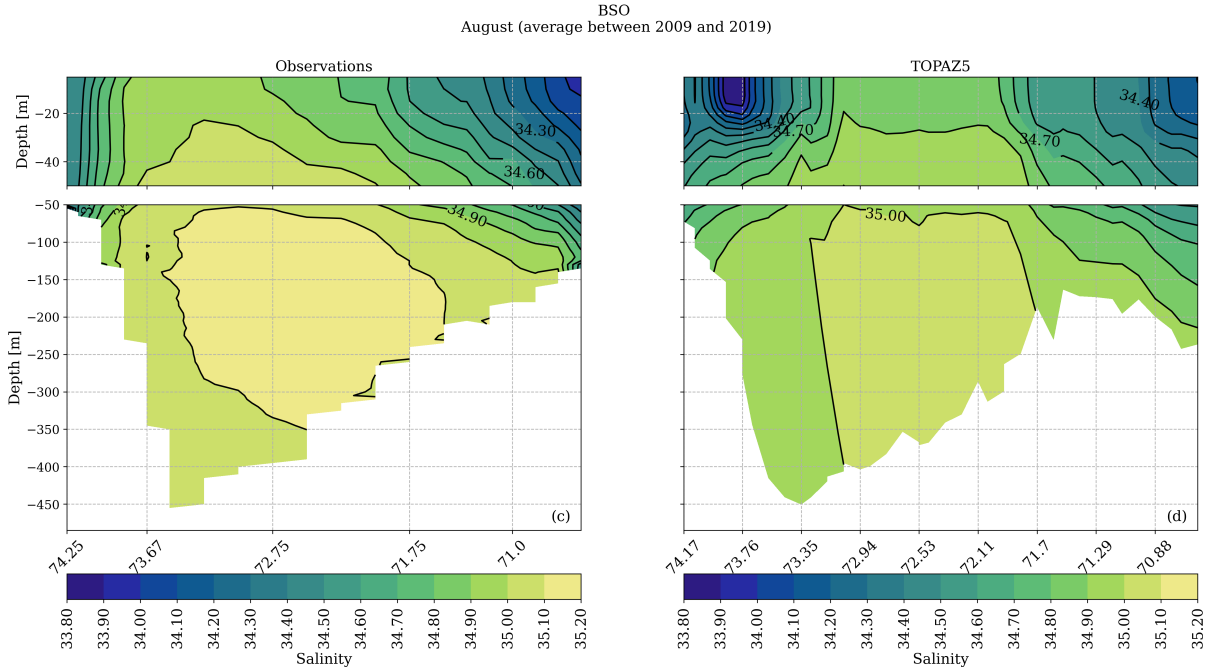

Fig. B2. Same as Fig. B1, but for August.

https://doi.org/10.5194/egusphere-2026-1520
Preprint. Discussion started: 8 May 2026

Appendix C. Data sources

The model forcing, initial conditions, and validation datasets are derived from publicly available data sources:

1. World Ocean Atlas 2018, temperature:
https://www.ncei.noaa.gov/access/world-ocean-atlas-2018/bin/woa18.pl (last access: April 2026).

2. World Ocean Atlas 2018, salinity:
https://www.ncei.noaa.gov/access/world-ocean-atlas-2018/bin/woa18.pl (last access: April 2026).

3. ERA5 atmospheric forcing data:
https://cds.climate.copernicus.eu/datasets/reanalysis-era5-single-levels?tab=download (last access: April 2026).

4. Global Ocean Physics Reanalysis GLORYS12V1:
https://data.marine.copernicus.eu/product/GLOBAL_MULTIYEAR_PHY_001_030/description (last access: April 2026).

5. OSTIA SST:
https://data.marine.copernicus.eu/product/SST_GLO_SST_L4_NRT_OBSERVATIONS_010_001/description#:~:text=https%3A//doi.org/10.48670/moi%2D00165 (last access: April 2026).

6. OSI SAF Global Ocean Sea Ice Concentration CDRs and ICDRs from PMW data (OSI-SAF):
https://doi.org/10.48670/moi-00136 (last access: April 2026).

7. CS2SMOS sea ice thickness:
The product can be downloaded from https://data.seaiceportal.de/data/cs2smos_awi/n/ (last access: April 2026).

8. Mixed Layer Depth climatology:
The MLD climatology is available on https://mld.ifremer.fr/Data_Description.php (last access: April 2026).

9. SLA from the Global Ocean Gridded Sea Surface Heights And Derived Variables product:
https://data.marine.copernicus.eu/product/SEALEVEL_GLO_PHY_L4_MY_008_047/description#:~:text=https%3A//doi.org/10.48670/moi%2D00148 (last access: April 2026).

https://doi.org/10.5194/egusphere-2026-1520
Preprint. Discussion started: 8 May 2026

Code and data availability

The source code is publicly available from the Nansen Environmental and Remote Sensing Centre repository at https://github.com/nansencenter/NERSC-HYCOM-CICE. The exact version of the TOPAZ5 model configuration used to produce the results presented in this paper is archived on Zenodo (https://doi.org/10.5281/zenodo.19230986; Othmani et al., 2026). The archive includes the model code, configuration and workflow scripts required to run the simulations. The model was compiled using the Intel Fortran compiler (ifort) and executed on the Betzy supercomputing system. Reproducibility requires access to a comparable high-performance computing environment.

The complete set of TOPAZ5 model outputs, analysis scripts, and figure-generation workflows is archived in the Norwegian Research Data Archive, NIRD RDA (https://doi.org/10.11582/2026.jrjkgirj; Othmani, 2026). All quantitative validation metrics and results presented in this paper are reproducible using the archived data.

Author contributions

AO prepared the article with contributions from all co-authors.

Competing interests

All authors declare no conflicts of interest.

Acknowledgments

This research has been supported by the Copernicus Marine Environment Monitoring Service (CMEMS) Arctic Marine Forecasting Centre (ARC MFC; Contract no. 21002L1). The computations were performed on the Norwegian Sigma2 infrastructure under project NS9481K.

https://doi.org/10.5194/egusphere-2026-1520
Preprint. Discussion started: 8 May 2026

Financial support

This research was funded by CMEMS, implemented by Mercator Ocean International under a delegation agreement with the European Union (grant no. 21002L1).

References

Beszczynska-Möller, A., Fahrbach, E., Schauer, U., and Hansen, E.: Variability in Atlantic water temperature and transport at the entrance to the Arctic Ocean, 1997–2010, ICES J. Mar. Sci., 69, 852–863, https://doi.org/10.1093/icesjms/fss056, 2012.

Bitz, C. M. and Lipscomb, W. H.: An energy-conserving thermodynamic model of sea ice, J. Geophys. Res., 104, 15669-15677, https://doi.org/10.1029/1999JC900100, 1999.

Bitz, C. M., Holland, M. M., Weaver, A. J., and Eby, M.: Simulating the ice-thickness distribution in a coupled climate model, J. Geophys. Res., 106, 2441–2463, https://doi.org/10.1029/1999JC000113, 2001.

Bleck, R.: An oceanic general circulation model in pressure coordinates, Ocean Model., 37, 55–88, https://doi.org/10.1016/S1463-5003(01)00012-9, 2002.

Buckley, M. W. and Marshall, J.: Observations, inferences, and mechanisms of Atlantic Meridional Overturning Circulation variability: A review, Rev. Geophys., 54, 5–63, https://doi.org/10.1002/2015RG000493, 2016.

Carrassi, A., Bocquet, M., Bertino, L., and Evensen, G.: Data assimilation in the geosciences: An overview of methods, issues, and perspectives, WIREs Clim. Change, 9, e535, https://doi.org/10.1002/wcc.535, 2018.

Counillon, F., Keenlyside, N., Bethke, I., Wang, Y., Billeau, S., Shen, M. L., and Bentsen, M.: Flow-dependent assimilation of sea surface temperature in isopycnal coordinates with the Norwegian Climate Prediction Model, Tellus A, 68, 32437, https://doi.org/10.3402/tellusa.v68.32437, 2016.

de Boyer Montégut, C., Madec, G., Fischer, A. S., Lazar, A., and Iudicone, D.: Mixed layer depth over the global ocean: An examination of profile data and a profile-based climatology, J. Geophys. Res. Oceans, 109, C12003, https://doi.org/10.1029/2004JC002378, 2004.

https://doi.org/10.5194/egusphere-2026-1520
Preprint. Discussion started: 8 May 2026

Docquier, D., Grist, J. P., Roberts, M. J., et al.: Impact of model resolution on Arctic sea ice and North Atlantic Ocean heat transport, Clim. Dyn., 53, 4989–5017, https://doi.org/10.1007/s00382-019-04840-y, 2019.

Donlon, C. J., Martin, M., Stark, J., Roberts-Jones, J., Fiedler, E., and Wimmer, W.: The Operational Sea Surface Temperature and Sea Ice Analysis (OSTIA) system, Remote Sens. Environ., 116, 140–158, https://doi.org/10.1016/j.rse.2010.10.017, 2012.

Dorn, W., Dethloff, K., Rinke, A., Frickenhaus, S., Gerdes, R., Karcher, M., and Kauker, F.: Sensitivities and uncertainties in a coupled regional atmosphere–ocean–ice model with respect to the simulation of Arctic sea ice, J. Geophys. Res., 112, D10118, https://doi.org/10.1029/2006JD007814, 2007.

Drévillon, M., Lellouche, J.-M., Régnier, C., Garric, G., Bricaud, C., Hernandez, O., and Bourdallé-Badie, R.: Quality information document for GLOBAL_REANALYSIS_PHY_001_030, CMEMS-GLO-QUID-001-030, Copernicus Marine Service, 2023.

Drinkwater, K. F., Sundby, S., and Wiebe, P. H.: Exploring the hydrography of the boreal/arctic domains of North Atlantic seas: Results from the 2013 BASIN survey, Deep-Sea Res. Pt. II, 180, 104880, https://doi.org/10.1016/j.dsr2.2020.104880, 2020.

Dukhovskoy, D. S., Morey, S. L., Martin, P. J., O'Brien, J. J., and Cooper, C.: Application of a vanishing, quasi-sigma vertical coordinate for simulation of high-speed, deep currents over the Sigsbee Escarpment in the Gulf of Mexico, Ocean Model., 28, 250–265, https://doi.org/10.1016/j.ocemod.2009.02.009, 2009.

Fine, E. C., McClean, J. L., Ivanova, D. P., Craig, A. P., Wallcraft, A. J., Chassignet, E. P., and Hunke, E. C.: Arctic ice-ocean interactions in an 8-to-2 km resolution global model, Ocean Model., 184, 102228, https://doi.org/10.1016/j.ocemod.2023.102228, 2023.

Groh, A., Horwath, M., Horvath, A., Meister, R., Sørensen, L. S., Barletta, V. R., Forsberg, R., Wouters, B., Ditmar, P., Ran, J., et al.: Evaluating GRACE mass change time series for the Antarctic and Greenland ice sheets, Geosciences, 9, 415, https://doi.org/10.3390/geosciences9100415, 2019.

Hassan, T., Allen, R. J., Liu, W., and Randles, C. A.: Anthropogenic aerosol forcing of the Atlantic meridional overturning circulation and the associated mechanisms in CMIP6 models, Atmos. Chem. Phys., 21, 5821–5846, https://doi.org/10.5194/acp-21-5821-2021, 2021.

https://doi.org/10.5194/egusphere-2026-1520
Preprint. Discussion started: 8 May 2026

Hersbach, H., Bell, B., Berrisford, P., Hirahara, S., Horányi, A., Muñoz-Sabater, J., et al.: The ERA5 global reanalysis, Q. J. R. Meteorol. Soc., 146, 1999–2049, https://doi.org/10.1002/qj.3803, 2020.

Hewitt, H. T., Roberts, M., Mathiot, P., et al.: Resolving and parameterising the ocean mesoscale in Earth system models, Curr. Clim. Change Rep., 6, 137–152, https://doi.org/10.1007/s40641-020-00164-w, 2020.

Hibler, W. D.: Modeling a variable thickness sea ice cover, Mon. Weather Rev., 108, 1943-1973, 1980.

Holte, J., Talley, L. D., Gilson, J., and Roemmich, D.: An Argo mixed layer climatology and database, Geophys. Res. Lett., 44, 5618–5626, https://doi.org/10.1002/2017GL073426, 2017.

Hordoir, R., Axell, L., Höglund, A., et al.: Nemo-Nordic 1.0: a NEMO-based ocean model for the Baltic and North seas – research and operational applications, Geosci. Model Dev., 12, 363–386, https://doi.org/10.5194/gmd-12-363-2019, 2019.

Hordoir, R., Skagseth, Ø., Ingvaldsen, R. B., et al.: Changes in Arctic stratification and mixed layer depth cycle: A modeling analysis, J. Geophys. Res. Oceans, 127, e2021JC017270, https://doi.org/10.1029/2021JC017270, 2022.

Hunke, E. C. and Dukowicz, J. K.: An elastic–viscous–plastic model for sea ice dynamics, J. Phys. Oceanogr., 27, 1849–1867, 1997.

Hunke, E. C., Lipscomb, W. H., Turner, A. K., Jeffery, N., and Elliott, S.: CICE: The Los Alamos sea ice model documentation and software user's manual, Version 5, Los Alamos National Laboratory, 2015.

Hunke, E. C.: Viscous–plastic sea ice dynamics with the EVP model: Linearization issues, J. Comput. Phys., 170, 18–38, https://doi.org/10.1006/jcph.2001.6710, 2001.

Iskandarani, M., Levin, J., Choi, B., and Haidvogel, D.: Comparison of advection schemes for high-order hp finite element and finite volume methods, Ocean Model., 10, 233–252, 2005.

Jiang, L., Duan, W., Wang, H., Liu, H., and Tao, L.: Evaluation of the sensitivity on mesoscale eddy associated with the sea surface height anomaly forecasting in the Kuroshio Extension, Front. Mar. Sci., 10, 1097209, https://doi.org/10.3389/fmars.2023.1097209, 2023.

https://doi.org/10.5194/egusphere-2026-1520
Preprint. Discussion started: 8 May 2026

Johnson, M., Proshutinsky, A., Aksenov, Y., et al.: Evaluation of Arctic sea ice thickness simulated by Arctic Ocean Model Intercomparison Project models, J. Geophys. Res., 117, C00D13, https://doi.org/10.1029/2011JC007257, 2012.

Juricke, S., Danilov, S., Koldunov, N. V., Oliver, M., and Sidorenko, D.: Ocean kinetic energy backscatter parametrization on unstructured grids: Impact on global eddy-permitting simulations, J. Adv. Model. Earth Syst., 12, e2019MS001855, https://doi.org/10.1029/2019MS001855, 2020.

Kara, A. B., Wallcraft, A. J., and Hurlburt, H. E.: A new solar radiation penetration scheme for use in ocean mixed layer studies: An application to the Black Sea using a fine-resolution hybrid coordinate ocean model (HYCOM), J. Phys. Oceanogr., 35, 13–32, https://doi.org/10.1175/JPO2677.1, 2005.

Large, W. G., McWilliams, J. C., and Doney, S. C.: Oceanic vertical mixing: A review and a model with a nonlocal boundary layer parameterization, Rev. Geophys., 32, 363–403, 1994.

Lien, V. S., Hjøllo, S. S., Skogen, M. D., Svendsen, E., Wehde, H., Bertino, L., Counillon, F., Chevallier, M., and Garric, G.: An assessment of the added value from data assimilation on modelled Nordic Seas hydrography and ocean transports, Ocean Model., 99, 43–59, https://doi.org/10.1016/j.ocemod.2015.12.010, 2016.

Lindström, G., Pers, C., Rosberg, J., Strömqvist, J., and Arheimer, B.: Development and testing of the HYPE (Hydrological Predictions for the Environment) water quality model for different spatial scales, Hydrol. Res., 41, 295–319, https://doi.org/10.2166/nh.2010.007, 2010.

Locarnini, R. A., Mishonov, A. V., Baranova, O. K., Boyer, T. P., Zweng, M. M., Garcia, H. E., Reagan, J. R., Seidov, D., Weathers, K. W., Paver, C. R., and Smolyar, I. V.: World Ocean Atlas 2018, Volume 1: Temperature, NOAA Atlas NESDIS 81, https://www.nodc.noaa.gov/, 2019.

Marshall, J. and Schott, F.: Open-ocean convection: Observations, theory, and models, *Rev. Geophys.*, **37**, 1-64, https://doi.org/10.1029/98RG02739, 1999.

Merryfield, W. J., Lee, W.-S., Wang, W., Chen, M., and Kumar, A.: Multi-system seasonal predictions of Arctic sea ice, Geophys. Res. Lett., 40, 1551–1556, https://doi.org/10.1002/grl.50317, 2013.

Nguyen, A. T., Pillar, H., Ocaña, V., Bigdeli, A., Smith, T. A., and Heimbach, P.: The Arctic Subpolar gyre sTate Estimate, J. Adv. Model. Earth Syst., 13, e2020MS002398, https://doi.org/10.1029/2020MS002398, 2021.

Notz, D. and Stroeve, J.: The trajectory towards a seasonally ice-free Arctic Ocean, Curr. Clim. Change Rep., 4, 407–416, https://doi.org/10.1007/s40641-018-0113-2, 2018.

Oki, T. and Sud, Y. C.: Design of the global river channel network for Total Runoff Integrating Pathways (TRIP), Earth Interact., 2, 1–37, 1998.

Othmani, A. Outputs and validation of TOPAZ5, a high-resolution ocean and sea-ice model for the Arctic and North Atlantic. [Data set]. NIRD RDA. https://doi.org/10.11582/2026.jrjkgirj, 2026.

Othmani, A., Samuelsen, A., Xie, J., Bertino, L., Mangini, F., and P. Raj, R. Model code and configuration for "TOPAZ5: A high-resolution ocean and sea-ice model for the Arctic and North Atlantic." (Version v1). Zenodo [model], https://doi.org/10.5281/zenodo.19230987, 2026.

Perovich, D., Smith, M., Light, B., and Webster, M.: Meltwater sources and sinks for multiyear Arctic sea ice in summer, The Cryosphere, 15, 4517–4525, https://doi.org/10.5194/tc-15-4517-2021, 2021.

Pickart, R. S., Spall, M. A., Ribergaard, M. H., Moore, G. W. K., and Milliff, R. F.: Deep convection in the Irminger Sea forced by the Greenland tip jet, *Nature*, 424, 152–156, https://doi.org/10.1038/nature01729, 2003.

Piunno, R., Moore, G. W. K., and Våge, K.: Impact of synoptic-scale atmospheric forcing conditions on deep convection in the Labrador Sea, *J. Geophys. Res.-Oceans*, 130, e2024JC021818, https://doi.org/10.1029/2024JC021818, 2025.

Raj, E. P., Chafik, L., Nilsen, J. E. Ø., Eldevik, T., and Halo, I.: The Lofoten Vortex of the Nordic Seas, Deep-Sea Res. I, 96, 1–14, https://doi.org/10.1016/j.dsr.2014.10.011, 2015.

Ricker, R., Hendricks, S., Kaleschke, L., Tian-Kunze, X., King, J., and Haas, C.: A weekly Arctic sea-ice thickness data record from merged CryoSat-2 and SMOS satellite data, The Cryosphere, 11, 1607–1623, https://doi.org/10.5194/tc-11-1607-2017, 2017.

Rudels, B. and Carmack, E.: Arctic Ocean water mass structure and circulation, Oceanography, 35, 52–65, https://doi.org/10.5670/oceanog.2022.116, 2022.

https://doi.org/10.5194/egusphere-2026-1520
Preprint. Discussion started: 8 May 2026

Sakov, P., Counillon, F., Bertino, L., Lisæter, K. A., Oke, P. R., and Korablev, A.: TOPAZ4: An ocean–sea ice data assimilation system for the North Atlantic and Arctic, Ocean Sci., 8, 633–656, https://doi.org/10.5194/os-8-633-2012, 2012.

Schubert, R., Vergara, O., and Gula, J.: The open ocean kinetic energy cascade is strongest in late winter and spring, Commun. Earth Environ., 4, 450, https://doi.org/10.1038/s43247-023-01111-x, 2023.

Selivanova, J., Iovino, D., and Cocetta, F.: Past and future of the Arctic sea ice in High Resolution Model Intercomparison Project climate models, The Cryosphere, 18, 2739–2763, https://doi.org/10.5194/tc-18-2739-2024, 2024.

Shi, J., Luo, B., Luo, D., et al.: Differing roles of North Atlantic oceanic and atmospheric transports in winter Eurasian Arctic sea-ice variability, npj Clim. Atmos. Sci., 7, 62, https://doi.org/10.1038/s41612-024-00605-5, 2024.

Smedsrud, L. H., Muilwijk, M., Brakstad, A., et al.: Nordic Seas heat loss, Atlantic inflow, and Arctic sea ice cover over the last century, Rev. Geophys., 60, e2020RG000725, https://doi.org/10.1029/2020RG000725, 2022.

Smedsrud, L. H., Sirevaag, A., Kloster, K., Sorteberg, A., and Sandven, S.: Recent wind driven high sea ice area export in the Fram Strait contributes to Arctic sea ice decline, The Cryosphere, 5, 821–829, https://doi.org/10.5194/tc-5-821-2011, 2011.

Smith, G. C., Hébert-Pinard, C., Gauthier, A.-A., et al.: Impact of assimilation of absolute dynamic topography on Arctic Ocean circulation, Front. Mar. Sci., 11, 1390781, https://doi.org/10.3389/fmars.2024.1390781, 2024.

Søiland, H., Chafik, L., and Rossby, T.: On the long-term stability of the Lofoten Basin Eddy, J. Geophys. Res. Oceans, 121, 4438–4449, https://doi.org/10.1002/2016JC011726, 2016.

Stammer, D.: Global characteristics of ocean variability estimated from TOPEX/POSEIDON altimeter measurements, J. Phys. Oceanogr., 27, 1743–1769, 1997.

Timmermans, M.-L. and Marshall, J.: Understanding Arctic Ocean circulation: A review of ocean dynamics in a changing climate, J. Geophys. Res. Oceans, 125, e2018JC014378, https://doi.org/10.1029/2018JC014378, 2020.

Turner, J., Bracegirdle, T. J., Phillips, T., Marshall, G. J., and Hosking, J. S.: An initial assessment of Antarctic sea ice extent in the CMIP5 models, J. Clim., 26, 1473–1484, https://doi.org/10.1175/JCLI-D-12-00068.1, 2013.

https://doi.org/10.5194/egusphere-2026-1520
Preprint. Discussion started: 8 May 2026

Volkov, D. L., Belonenko, T. V., and Foux, V. R.: Puzzling over the dynamics of the Lofoten Basin, Geophys. Res. Lett., 40, 738–743, https://doi.org/10.1002/grl.50126, 2013.

Wang, Q., Wekerle, C., Danilov, S., Wang, X., and Jung, T.: A 4.5 km resolution Arctic Ocean simulation with the global multi-resolution model FESOM 1.4, Geosci. Model Dev., 11, 1229–1255, https://doi.org/10.5194/gmd-11-1229-2018, 2018.

Weijer, W., Cheng, W., Drijfhout, S. S., Fedorov, A. V., Hu, A., Jackson, L. C., et al.: Stability of the Atlantic Meridional Overturning Circulation: A review and synthesis, J. Geophys. Res. Oceans, 124, 5336–5375, https://doi.org/10.1029/2019JC015083, 2019.

Woodgate, R. A., Aagaard, K., and Weingartner, T. J.: Interannual changes in the Bering Strait fluxes of volume, heat, and freshwater, Geophys. Res. Lett., 33, L15609, https://doi.org/10.1029/2006GL026931, 2006.

Xie, J., Bertino, L., Counillon, F., Lisæter, K. A., and Sakov, P.: Quality assessment of the TOPAZ4 reanalysis in the Arctic over the period 1991–2013, Ocean Sci., 13, 123–144, https://doi.org/10.5194/os-13-123-2017, 2017.

Yashayaev, I.: Intensification and shutdown of deep convection in the Labrador Sea were caused by changes in atmospheric and freshwater dynamics, *Commun. Earth Environ.*, **5**, 156, https://doi.org/10.1038/s43247-024-01296-9, 2024.

Zalesak, S.: Fully multidimensional flux-corrected transport algorithms for fluids, J. Comput. Phys., 31, 335–362, 1979.

Zhou, S., Renfrew, I. A., and Zhai, X.: The impact of stochastic mesoscale weather systems on the Atlantic Ocean, J. Clim., 36, 791–804, https://doi.org/10.1175/JCLI-D-22-0044.1, 2023.

Zweng, M. M., Reagan, J. R., Seidov, D., Boyer, T. P., Locarnini, R. A., Garcia, H. E., Mishonov, A. V., Baranova, O. K., Weathers, K. W., Paver, C. R., and Smolyar, I. V.: World Ocean Atlas 2018, Volume 2: Salinity, NOAA Atlas NESDIS, 82, NOAA, 2019.